Computers and Chemical Engineering 199 (2025) 109151

Contents lists available at ScienceDirect

Computers and Chemical Engineering

journal homepage: www.elsevier.com/locate/compchemeng

Integrated thermo-economic organic Rankine cycle and working fluid design – On the accuracy of molecular-based computer-aided methodologies

Matthias Mersch [a,b,c], Dominik Tillmanns [d], Paul Sapin [a,c], Johannes Schilling [d,e], André Bardow [d,e,f], Christos N. Markides [a,c,*]

[a] Clean Energy Processes (CEP) Laboratory, Department of Chemical Engineering, Imperial College London, London SW7 2AZ, UK
[b] Centre for Environmental Policy, Imperial College London, London SW7 2AZ, UK
[c] The Sargent Centre for Process System Engineering, Department of Chemical Engineering, Imperial College London, London SW7 2AZ, UK
[d] Institute of Technical Thermodynamics, RWTH Aachen University, Schinkelstraße 8, 52062 Aachen, Germany
[e] Energy and Process Systems Engineering, ETH Zurich, Tannenstrasse 3, 8092 Zurich, Switzerland
[f] Institute of Energy and Climate Research – Energy Systems Engineering – Forschungszentrum Jülich GmbH, Wilhelm-Johnen-Straße, 52425 Jülich, Germany

ARTICLE INFO

Keywords:
Computer-aided molecular and process design
Organic rankine cycle
Thermo-economic optimisation
Uncertainty
Waste-heat recovery
Working fluid

ABSTRACT

The performance of Organic Rankine cycle (ORC) systems is defined by the system design as well as working fluid selection. Integrated thermo-economic optimisation of both can unlock maximum system potential in terms of power generation at a minimal cost. However, such optimisation is associated with uncertainties related to the underlying thermodynamic fluid models, ORC system models, and equipment cost correlations. In this paper, the main sources of uncertainty are quantified and their impact on optimal system design and working fluid selection is analysed. A computer-aided molecular and process design (CAMPD) optimisation framework based on first-law system design models is developed and validated with experimental data. Results reveal that the developed framework can identify promising working fluid candidates with high probabilities, even considering the most important sources of uncertainty. In a case study of industrial waste-heat utilisation, it was found that while uncertainties challenge the strict discrimination of the most promising working fluids, they mainly affect absolute performance values, rather than the overall ranking of working fluids. Propane was identified as having a 94-% probability of being among the best 3 working fluids. Furthermore, although the overall specific investment costs are highly uncertain (mean: 3810 £/kW, standard deviation: 720 £/kW), the results are less sensitive to uncertainties in fluid equilibrium and transport properties (standard deviation: 160 £/kW), with the impact of equipment cost uncertainties being dominant. The analysis of uncertainties in working fluid selection also applies to other CAMPD problems, and other applications of group-contribution-based equations of state.

1. Introduction

Organic Rankine cycle (ORC) systems can generate electricity from low-temperature heat sources, such as solar, geothermal, or waste heat (Markides and Wang, 2023; Handagama et al., 2023). However, careful design of an ORC system, its equipment and working fluid is necessary to achieve high efficiencies and low costs. Integrated thermo-economic optimisations of system and working fluid have proven useful in designing ORC systems (Schilling et al., 2017a; White et al., 2018). However, the methodology is subject to various sources of uncertainty, such as fluid models, equipment models, and cost correlations.

The working fluid choice substantially influences the performance of ORC systems (Stijepovic et al., 2012). The selection of the optimal working fluid is challenging due to the large number of potential working fluids and the variety of operating conditions, such as heat source temperatures (Linke et al., 2015). The working fluid selection challenge has become even more critical with the ratification of the Kigali Amendment to the Montreal Protocol, which aims to phase out high-GWP (global warming potential) hydrofluorocarbons, widely used as working fluids for ORC systems (United Nations, 2016). Hydrocarbons have emerged as a potentially promising replacement, but the variety of applications makes it impossible to find a general solution to the working fluid selection problem. Instead, optimisation should be

* Corresponding author.
E-mail address: c.markides@imperial.ac.uk (C.N. Markides).

https://doi.org/10.1016/j.compchemeng.2025.109151
Received 20 January 2025; Received in revised form 21 March 2025; Accepted 13 April 2025
Available online 14 April 2025

Nomenclature

Abbreviations

BPHEX	Brazed-plate heat exchanger
CAMD	Computer-aided molecular design
CAMPD	Computer-aided molecular and process design
EOS	Equation of state
GC	Group-contribution
HEX	Heat exchanger
LCOE	Levelised cost of energy
MINLP	Mixed-integer non-linear program
ORC	Organic Rankine cycle
PC-SAFT	Perturbed-chain statistical associating fluid theory
SAFT	Statistical associating fluid theory
SRK	Soave-Redlich-Kwong
std	Standard deviation

Greek symbols

α	Convective heat transfer coefficient (W/m/K)
β	Chevron angle
Δ	Difference
ε/k	Segment dispersion energy (K)
η	Efficiency
ρ	Density (kg/m^3)
σ	Segment diameter (m, Å)
χ	Vapour quality

Latin symbols

A	Area (m^2)
f	Objective function
g_i	Equality constraints
h_i	Inequality constraints
h	Specific enthalpy (J/kg)
k_i	Molecular feasibility constraints
k	Thermal conductivity (W/m/K)
l_{cor}	Plate corrugation (m)
m	Segment number
$\dot{m}$	Mass flowrate (kg/s)
Nu	Nusselt number
p	Pressure (Pa)
Pr	Prandtl number
$\dot{Q}$	Heat flow rate (W)
Re	Reynolds number
r_p	Pressure ratio
s	Specific entropy (J/kg/K)
T	Temperature (K)
U	Overall heat transfer coefficient (W/m/K)
$\dot{W}$	Power (W)
x	Continuous optimisation variables
y	Discrete optimisation variables

Subscripts & superscripts

A, B	Sides of heat exchanger
cond	Condenser/condensation
cw	Cooling water
evap	Evaporator/evaporation
exp	Expander/expansion
gen	Generator/generation
hs	Heat source
i	Index
in	Inlet
l	Liquid
max	Maximum
meas	Measured
min	Minimum
out	Outlet
pred	Predicted
pump	Pump/pumping
sc	Subcooling
sh	Superheating
v	Vapour
wf	Working fluid
crit	Critical
is	Isentropic
mech	Mechanical
r	Reduced
syn	Synthetic

performed for each application (Bao and Zhao, 2013).

Conventionally, working fluid selection and system design are performed in two steps: First, a database of working fluid candidates is screened, using heuristic and/or analytical methods to pre-select fluids. In the second step, the system is optimised for each of the pre-selected fluids and the working fluid & system combination that performs best is selected. Studies applying this methodology to ORC systems have been conducted for a multitude of applications, such as co-generation biomass plants (Drescher and Brüggemann, 2007), solar desalination plants (Delgado-Torres and García-Rodríguez, 2010), solar power plants (Tchanche et al., 2009), geothermal power plants (Saleh et al., 2007; Zhai et al., 2014), and waste-heat recovery applications (Wang et al., 2011; Preißinger et al., 2017; Pantaleo et al., 2019; Chatzopoulou et al., 2019).

Stijepovic et al. (2012) conducted an analysis concluding that four working fluid properties (molar mass, compressibility factor, ideal gas heat capacity, liquid density) are relevant for the thermodynamic performance of ORC systems, while five additional properties (liquid specific heat capacity, heat of evaporation, critical pressure, liquid thermal conductivity, vapour density) need to be considered for the economic performance. However, the properties show trade-offs regarding performance and the work did not rigorously screen working fluids. Chen et al. (2010) reviewed working fluid selection criteria and an evaluation of 35 fluids, concluding that the critical temperature and the "dryness" ds/dt are essential parameters. Quoilin et al. (2011) performed a comprehensive thermo-economic optimisation of a small-scale ORC system for waste heat recovery applications, using heuristic criteria to pre-select eight working fluid candidates. The study highlighted that thermodynamic and thermo-economic optimisations might lead to different results. Freeman et al. (2017) studied working fluids for domestic solar-ORC systems, using detailed models of solar collectors and considering a year-round operation. A range of hydrocarbons and halogenated refrigerants were investigated in that study. Andreasen et al. (2014) considered all pure fluids and predefined mixtures with zero ozone depletion potential from the NIST REFPROP database as well as binary mixtures of pure fluids in their working fluid selection. Schwöbel et al. (2017) used the COSMO-RS model to conduct a high-throughput screening of the PubChem chemical structure database containing more than 72 million entries. After an initial filtering, thermodynamic properties were determined for over 2 million structures. Based on that, about 3000 were selected as working fluid candidates and ranked by thermal efficiency. Emadi et al. (2020) performed a thermo-economic, multi-objective optimisation of a dual-loop ORC system recovering waste heat from a fuel cell, using an artificial neural network to predict the system performance. They considered a total of nine refrigerants. None of these studies considered the impact of

uncertainties on the fluid selection.

The two-step methodology with a heuristic working fluid pre-selection followed by a system design optimisation may inadvertently exclude promising fluids and therefore lead to suboptimal results. Hence, an integrated, single-step optimisation that simultaneously considers working fluid and systems design is recommended (Linke et al., 2015; Quoilin et al., 2013). This integrated optimisation is interpreted as a computer-aided molecular and process design (CAMPD) problem (Markides et al., 2025).

CAMPD combines thermodynamic or thermo-economic system models with methods to determine thermophysical properties of substances (i.e., the working fluid) from their molecular structure, often expressed via functional groups. This problem typically results in mixed-integer non-linear programming (MINLP) formulations comprising continuous process variables and discrete variables to describe the working fluid molecules (Gani, 2004). CAMPD requires models to compute thermophysical properties from fluid-specific parameters and molecular structure. Equations of state (EOSs) are most frequently used for the identification of organic working fluids, other options are quantum-mechanics models, excess Gibbs energy models, and artificial intelligence approaches. Widely used classes of EOSs in CAMPD are cubic EOSs, such as the Peng-Robinson EOS (Peng and Robinson, 1976; Liang et al., 2022) or the Soave-Redlich-Kwong (SRK) EOS (Soave, 1972), and derivates of the statistical associating fluid theory (SAFT) (Chapman et al., 1989), such as SAFT-VR Mie (Lafitte et al., 2013) or perturbed-chain SAFT (PC-SAFT) (Gross and Sadowski, 2001).

Papadopoulos et al. (2010) identified limitations of working fluid screenings and proposed a CAMPD methodology based on the Peng-Robinson EOS, iteratively altering the molecular structure of the working fluid. The authors showed that substances not included in databases have a high potential for ORC systems, thus justifying the CAMPD approach. The framework was later extended to design working fluid mixtures (Papadopoulos et al., 2013). The latter study also included a sensitivity analysis to investigate the influence of uncertainties in the boiling temperature, critical temperature, and critical pressure of the mixtures. Different mixtures were shown to exhibit different sensitivities, even if they show similar nominal performance. Palma-Flores et al. (2015) used a CAMPD approach to identify promising working fluids for low-temperature heat recovery applications, considering a comprehensive set of 39 functional groups. Rather than optimising the power output or the costs of the ORC system, four working fluid parameters considered beneficial for working fluids were used as objective functions. White et al. (2017) performed a CAMPD-based integrated working fluid and system optimisation, using the SAFT-γ Mie EOS with group-contribution (GC) methods. In addition to ORC parameters such as pressure levels and the degree of superheating, the chain length of n-alkanes, methyl alkanes, 1-alkenes and 2-alkenes was optimised. The framework was later extended to: (i) a thermo-economic assessment, identifying optimal working fluids depending on the heat source temperatures (White et al., 2018); and (ii) a multi-objective optimisation, investigating trade-offs between investment costs and power output (van Kleef et al., 2019). Bowskill et al. (2020) conducted a CAMPD optimisation of the net power output of ORC systems using the SAFT-γ Mie EOS. The authors considered linear alkane and alkene groups as well as various oxygen groups for a total of ~59,000 feasible chemical structures. Lampe et al. (2015) used a continuous-molecular targeting CAMD (CoMT-CAMD) approach (Bardow et al., 2010) for a two-stage integrated working fluid and system optimisation based on the group-contribution PC-SAFT EOS. The first step identifies a hypothetical, optimal working fluid mapped to existing molecules in the second step. Schilling et al. (2017b) combined these two steps into a single-stage framework, achieving a more accurate identification of optimal working fluids. Combined with PC-SAFT-based transport property models as well as equipment design and cost correlations, the framework was later used for integrated thermo-economic working fluid and system optimisations (Schilling et al., 2017a). Most recently, Liang et al. (2022) presented an MINLP superstructure optimisation of ORC systems, using an iterative solution methodology to handle the complexity of the problem.

The thermo-economic working fluid and system optimisation is subject to various uncertainties: The thermophysical equilibrium property values predicted by EOSs differ from the actual values, and the thermodynamic cycle and equipment models provide only approximations of the performance of real machines. Additional sources of uncertainty are, e.g., the transport properties, the operating conditions, and the investment, operating and maintenance costs. Though many articles have been published on ORC working fluid and system design, these uncertainties were typically neglected or only considered in a simplified way.

Papadopoulos et al., 2013 proposed a non-linear sensitivity analysis on previously determined Pareto-optimal working fluid mixtures. Schilling et al. (2017a) conducted a post-optimality Monte Carlo study, considering uncertainties in the thermophysical properties calculated from the PC-SAFT EOS. They found that even though the objective value distributions of the two best working fluids largely overlap, CAMPD optimisation can still provide valuable working fluid performance rankings. Tillmanns et al. (2022) used a similar framework to optimise ORC-based pumped-thermal electricity storage system. The authors only analysed the impact of compressor cost correlations and found that the specific investment costs of the optimal system change by -42 % and +31 % depending on the correlation used. Zhang et al. (2020) investigated the prediction accuracy of PC-SAFT for siloxanes by comparing fluid properties calculated using PC-SAFT with values from NIST REFPROP. As usual, the SAFT parameters were fitted to liquid density and vapour pressure data. The average relative deviations between PC-SAFT and REFPROP for these properties were in the range from 0.6 to 2.8 %. The fitted parameters were then used to calculate deviations in compressibility factor, isobaric heat capacity and volume expansion coefficient, which were in the range from 1.1 to 18 %. The authors also determined the deviations in enthalpy and entropy in the superheated vapour phase, finding that the average relative deviations were below 0.6 %. It was shown that for high-temperature ORC systems with siloxanes as working fluid, the deviations in the predicted performance between PC-SAFT and REFPROP are smaller than 3 % for most of the considered range of operating conditions.

Frutiger et al. (2016a, 2016b, 2017, 2018, 2019) have significantly contributed to the parameter estimation and uncertainty analysis of EOSs. Rather than applying the uncertainties to the outputs of the EOS (i.e., the thermophysical properties), the authors determined the uncertainties in the EOS input parameters. First, the authors developed a methodology to estimate GC-parameters and associated uncertainties from experimental data for a heat of combustion model (Frutiger et al., 2016a). A bootstrap method, described in Section 4.1, was found to be a valid method to analyse uncertainties if the underlying distribution is unknown. It was also concluded that the GC-method had parameter identifiability issues indicated by significant correlations between parameters. However, the developed methodology was found to still be highly valuable in predicting thermophysical fluid properties from molecular structures.

Frutiger et al. (2017) then applied the bootstrap method to estimate uncertainty distributions of the SRK and the PC-SAFT EOS parameters for cyclopentane. The parameter distributions determined this way were then used to analyse the performance of an ORC system using cyclopentane as the working fluid. A Latin hypercube parameter sampling, based on the estimated parameter distributions and accounting for correlations between parameters, was used to generate a set of 250 input parameter combinations. Then, the ORC system model was solved for each sample. The standard deviations in net power outputs were 1 % and 0.2 % for the PC-SAFT and SRK EOSs, respectively. The results were found to be significantly more sensitive to the EOS parameters than the parameters of the heat capacity model. The work only considered cyclopentane as a working fluid and did not perform a CAMPD

optimisation. Other uncertainties unrelated to the EOSs were not considered.

In a related study, Frutiger et al. (2016b) also investigated the role of uncertainties in a working fluid screening using the Peng-Robinson EOS. Uncertain EOS input parameter distributions were estimated and sampled as in the previous study (Frutiger et al., 2017), and the ORC system model was solved for each sample and each of the considered working fluids, 1965 in total. The working fluid candidates were ranked and confidence intervals for the net power output were provided. For mean values of 1040 to 1150 kW, the confidence intervals were small (< 15 kW) for non-halogenated fluids such as isobutane, but very large (up to 900 kW) for complex, halogenated fluids. The authors concluded that the working fluid ranking based on mean values or uncertainties can significantly differ and studies investigating working fluids for ORC systems should account for uncertainties. Frutiger et al. (2019) then applied a Monte Carlo based optimisation approach to account for uncertainties in the SRK EOS in the CAMD optimisation of an ORC for marine applications. The authors considered uncertainties in the GC parameters and performed the CAMD optimisation for 250 random samples, maximising the net power output of the ORC. They highlighted differences between a robust solution minimising risk versus an optimistic solution that yields better performance in some cases but has a higher risk of low performance. Jones et al. (2019) conducted a similar analysis for a heat pump (maximising the COP) and a molecular distillation, using a fixed working fluid, and performed sensitivity analyses. They concluded that the results were most sensitive towards uncertainty in the acentric factor of the working fluid, which is a key input to the SRK EOS. Frutiger et al. (2018) also maximised the COP of a heat pump considering uncertainties in the SRK EOS, performing a CAMD optimisation to identify the optimal working fluid. The authors showed that the ranges of COP are much smaller for some working fluids compared to others, which is favourable for a conservative choice of working fluid. None of these studies considered uncertainties beyond those of the SRK EOS.

This work presents an integrated thermo-economic optimisation of ORC system and working fluid using the PC-SAFT EOS. Experimentally validated thermo-economic equipment models are used to estimate the performance of the ORC system with different working fluids. Uncertainties in the EOS, the transport property models, and equipment cost correlations are quantified and explicitly considered in the optimisation and their influence on the optimal system design and working fluid is analysed. This integrated methodology with explicit consideration of uncertainties in the CAMPD optimisation represents a key novelty, as studies in literature are limited to only one working fluid, only consider fewer sources of uncertainty and typically only a posteriori after the optimisation, and/or do not include any optimisation. Furthermore, using an experimentally validated process model is a key novelty. While this study focusses solely on ORC systems, similar system and working fluid design problems arise for heat pumps, chillers, or absorption systems.

The article is structured as follows: Section 2 presents the methodology and relevant working fluid and ORC system models, Section 3 contains a validation of the models against experimental data obtained from an ORC system test facility, Section 4 outlines the methodology to quantify and account for uncertainties, Section 5 discusses the results of the study, and Section 6 provides concluding remarks.

2. Integrated thermo-economic system and working fluid optimisation framework

The developed optimisation framework combines thermo-economic models of an ORC system with the homo-segmented group-contribution method of the PC-SAFT EOS (Gross and Sadowski, 2001) to calculate thermophysical fluid properties from molecular structures. This setup facilitates a simultaneous CAMPD optimisation of process variables and working fluid. The problem formulation is based on the methodology developed by Schilling et al. (2017a, 2017b). The resulting MINLP optimisation problem is described by:

$$\min_{x,y} f(x,y)$$

subject to

$$g_i(x,y) = 0 \text{ equipment models}$$

$$h_i(x,y) \leq 0 \text{ equipment limits} \quad (1)$$

$$k_i(y) = 0 \text{ molecular feasibility}$$

$$x_{\min} \leq x_i \leq x_{\max} \in \mathbb{R}^n \text{ bounds on continuous variables}$$

$$y_{\min} \leq y_i \leq y_{\max} \in \mathbb{Z}^m \text{ bounds on discrete variables}$$

The objective function f depends on the continuous variables x and the discrete variables y. The objective can be, e.g., to maximise the power output in a thermodynamic optimisation, or to minimise the specific investment costs in a thermo-economic optimisation. The continuous decision variables x represent the system design degrees of freedom, while the discrete decision variables y describe the molecular structure of the working fluid (see Section 2.2). The thermodynamic cycle and equipment models (see Section 2.1) result in a set of equality constraints g_i, while equipment limits are enforced via inequality constraints h_i. The molecular feasibility constraints k_i ensure that only chemically feasible molecules are considered (see Struebing (2011)). Additionally, all decision variables are bound to limit values to reasonable ranges.

The optimisation framework, thermodynamic cycle and equipment models are implemented in MATLAB, while the fluid calculations are implemented in Python, as they are based on an open-source Python library implementing PC-SAFT (Baird, 2020). The optimisation problem is solved using MATLAB's surrogate optimisation algorithm, which is a stochastic solver designed for global optimisation of complex, non-linear objective functions (The MathWorks Inc. 2021). Once the MINLP solver identifies the optimal working fluid, the optimum is refined using an interior-point non-linear optimisation solver (The MathWorks Inc. 2021). The models are presented in the following sections.

2.1. Thermodynamic ORC system models

ORC systems utilise a thermodynamic cycle that, in its simplest form, consists of four steps, as shown in Fig. 1: using electricity ($\dot{W}_{\text{pump}}$), a pump increases the pressure of a liquid working fluid ($\dot{m}_{\text{wf}}$) from a lower pressure level (p_{cond}) to a higher pressure level (p_{evap}). The high-pressure working fluid is then evaporated and superheated (ΔT_{sh}) in an evaporator, using heat ($\dot{Q}_{\text{hs}}$) from a heat source. The high-pressure working fluid vapour is then expanded through the expander, generating power ($\dot{W}_{\text{gen}}$) in the process. Finally, the working fluid is condensed and subcooled (ΔT_{sc}) in the condenser, rejecting heat ($\dot{Q}_{\text{cw}}$) to the cooling water.

Advanced ORC system concepts may involve, e.g., an additional heat exchanger acting as a recuperator, or supercritical fluid states. However, only subcritical, non-recuperated ORC systems are modelled in this work.

2.1.1. ORC system model

Quasi-steady operation of all equipment is assumed in the ORC system model, and potential and kinetic energy terms are neglected. Further, following an analysis that showed that typical pressure losses of 20–70 kPa expected in the evaporator and condenser (Alfa Laval, 2025) result in a 2–6 % reduction in the net power output, which is small compared to the impact of the various uncertainties considered in this paper, it is assumed in line with similar modelling attempts in the literature (Schilling et al., 2017a; Papadopoulos et al., 2010; van Kleef et al., 2019; Bowskill et al., 2020; Thierry et al., 2016) that the effects of

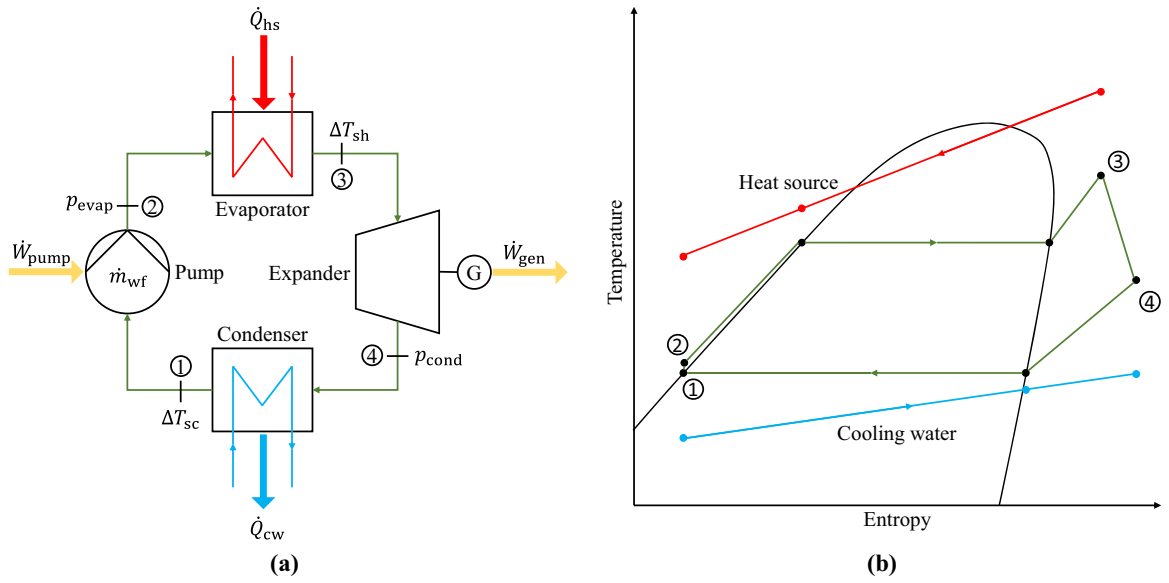

Fig. 1. (a) Flowsheet of a simple ORC system; and (b) ORC on a temperature-entropy diagram. The temperatures of the heat source and cooling water stream are shown in (b) for illustrative purposes.

pressure losses in piping and heat exchangers are negligible.

The non-recuperated ORC typically has five degrees of freedom: the two pressure levels p_{evap} and p_{cond}, two temperatures defined by the superheating ΔT_{sh} and subcooling ΔT_{sc}, and the working fluid mass flowrate $\dot{m}_{wf}$. It is assumed that the working fluid is saturated at the condenser outlet ($\Delta T_{sc} = 0$), as subcooling only reduces the thermal efficiency of the cycle. However, ensuring that the working fluid is fully condensed at the pump inlet is vital to avoid damage. The remaining four degrees of freedom are selected as the continuous decision variables for the optimisation:

$$x = \left\{p_{evap}^{r},\ p_{cond}^{r}, \Delta T_{sh},\ \dot{m}_{wf}\right\}. \tag{2}$$

The evaporation and condensation pressure levels are expressed via reduced pressures, defined as ratio of absolute pressure to critical pressure $p_i^{r} = p_i/p^{crit}$, to ensure subcritical operation via a strict upper bound in the optimisation problem formulation. Further details on the ORC system model and relevant equations are provided in Section S6 in the supplementary information.

In addition to the thermodynamic cycle equations, several inequality constraints are imposed by the system:

- The minimum approach temperature in the evaporator and condenser must not be violated.
- The evaporation pressure must be higher than the condensation pressure.
- The maximum pressure is limited to 50 bar to avoid unreasonably high pressures that would require specialised equipment.
- The minimum pressure is limited to 1 bar to eliminate the risk of ambient air leaking into the system.

Additionally, the upper and lower bounds shown in Table 1 are imposed on the decision variables. The upper bound of the working fluid mass flowrate is varied depending on the parameters of the case study. This ensures the scalability of the model, while the search space for the optimiser is smaller compared to just setting an arbitrary large upper bound. It is never reached in the optimal solutions presented in this work, and therefore does not affect the results.

In this study, the vapour quality at the expander outlet is not constrained. The expander is assumed to be a scroll machine which, unlike turbomachines, can handle two-phase expansion without damage (Lemort et al., 2013).

2.1.2. Equipment models

Thermodynamic models have been developed for each of the four main equipment items of the ORC system. Lumped models based on the isentropic efficiency are used for the expander and pump. First, the working fluid outlet state is calculated for the isentropic case:

$$h_{out}^{is} = h(p_{out}, s_{in}). \tag{3}$$

Then, the enthalpy of the actual outlet state is determined from the isentropic efficiency:

$$\begin{aligned} h_{pump,out} &= h_{pump,in} + \frac{h_{pump,\ out}^{is} - h_{pump,in}}{\eta_{pump}^{is}}, \\ h_{exp,out} &= h_{exp,in} - \eta_{exp}^{is}\left(h_{exp,in} - h_{exp,out}^{is}\right). \end{aligned} \tag{4}$$

In these equations, p denotes pressures, h specific enthalpies, s specific entropies, and η efficiencies. The subscripts identify pump and expander inlets and outlets, while the superscript "is" indicates isentropic states. The isentropic efficiency η^{is} is either assumed to be a fixed value or determined from experimental performance maps (see Section S8 in the supplementary information). The respective electrical input or output power is then calculated from the enthalpy difference, the mass flowrate, and the mechanical/electrical efficiency, which is assumed to

Table 1
Upper and lower bounds enforced on continuous decision variables in the optimisation.

x_{min}	x	x_{max}	Explanation
0.01	p_{evap}^{r}	0.8	Enforce subcritical cycle – fluid models become unreliable and operation difficult close to the critical point.
0.01	p_{cond}^{r}	0.8	
0 K	ΔT_{sh}	100 K	Limit the degree of superheating.
0.01 kg/s	$\dot{m}_{wf}$	$\min(\dot{m}_{hs}, \dot{m}_{cw})$	Limit working fluid mass flowrate.

be 95 %.

The evaporator and condenser are modelled as brazed-plate heat exchangers (BPHEX). Opposed to the expander and pump models, the BPHEX model is spatially resolved. The heat exchanger (HEX) is divided into three regions based on the working fluid flow regime: liquid flow (preheating/subcooling), two-phase flow (evaporation/condensation) and vapour flow (superheating/precooling). Each region is then discretised, and heat transfer equations are solved for each incremental HEX section. The mass flow is assumed to be equally distributed between the BPHEX channels.

Several heat transfer correlations were considered and validated against experimental data. Details are provided in Section 3 and Section S7 in the supplementary information. Single-phase heat transfer is modelled using the correlation of Bogaert and Böles (1995) for Reynolds numbers below 1000 and the correlation of Chisholm and Wanniarachchi (1991) for Reynolds numbers above 1000. An asymptotic correlation is used to model evaporative heat transfer, while the correlation of Thonon and Bontemps (2002) is used to model heat transfer during condensation.

Sizing and, therefore, costing the heat exchangers requires the BPHEX geometry. The design problem has four degrees of freedom: The plate height and width, the number of plates and the plate spacing. The geometry is determined using the following four constraints:

1. Total area: The required area is calculated from the discretised heat transfer model described above.
2. Maximum flow velocity: The fluid velocity in the channels is limited to 3 m/s for liquid flow and 7.6 m/s for vapour flow, which are industry standard values (Deppmann, 2025).
3. Plate spacing: The plate spacing of BPHEX is typically between 1.5 to 7 mm (Shah and Sekuli, 2003).
4. Height/width ratio: Ratio fixed to 4/1 to obtain realistic dimensions.

Further details on the BPHEX model and the heat transfer correlations considered in this work, including relevant equations, are provided in Section S9 in the supplementary information.

2.2. Working fluid thermophysical property calculations

For the CAMPD optimisation, the working fluid is represented by its functional groups. These functional groups are then used to calculate the thermophysical fluid properties required for the system model from an EOS using a group-contribution (GC) approach. For this work, we follow the approach of Schilling et al. (2017a). All thermodynamic equilibrium properties are calculated from the PC-SAFT EOS (Gross and Sadowski, 2001). For unpolar, non-associating molecules, PC-SAFT calculates residual thermodynamic properties from three molecular pure component parameters: the segment number m, the segment diameter σ and the segment dispersion energy ε/k (Schilling et al., 2017a). In the GC approach, the molecular SAFT parameters are calculated from the parameters of the individual functional groups. Here, a homosegmented GC approach is used, applying the mixing rules of Vijande et al. (2004). The PC-SAFT parameters of the functional groups are taken from Sauer et al. (2014), who fitted them to experimental liquid density and vapour pressure data of many organic fluids.

Since PC-SAFT only calculates residual thermodynamic properties, a reference is required to determine absolute properties. In line with many publications using PC-SAFT, the ideal gas heat capacity is selected as reference and calculated from Joback & Reid's polynomial GC approach (Joback and Reid, 1987).

In addition to the thermodynamic equilibrium properties, thermo-economic models also require transport properties (viscosity and thermal conductivity) to size equipment. Recently developed models based on Rosenfeld's entropy scaling (Rosenfeld, 1977; Rosenfeld, 1999) enable the calculation of transport properties from PC-SAFT. Lötgering-Lin and Gross (2015) developed a GC approach for the viscosity, and Hopp and Gross (2017) for the thermal conductivity. These models allow for thermodynamically consistent modelling of fluid equilibrium and transport properties.

Six organic functional groups are considered for this study. The number of occurrences (#) of each group are the discrete optimisation variables that describe the working fluid:

$$y = \{\#-\mathrm{CH_3}, \#-\mathrm{CH_2}-, \#>\mathrm{CH}-, \#>C<, \#=\mathrm{CH}-, \#=\mathrm{CH_2}\}. \tag{5}$$

These functional groups allow the creation of a multitude of linear and branched alkanes and alkenes. The framework can be extended to additional functional groups if the GC parameters are available.

All properties of water, which is used to cool the condenser and as the heat source in some cases, are calculated using CoolProp (Bell et al., 2014), which is based on a Helmholtz EOS. In other cases, a thermo-oil is used to transfer heat from the source to the ORC system. The properties of the oil are calculated from the datasheet (Olefins and Surfactants, 2003).

2.3. Equipment costing

For thermo-economic optimisations, estimating the plant costs is necessary to calculate economic performance indicators, such as the specific investment cost or the net present value. The latter is more useful to make investment decisions, but it requires assumptions on, e.g., electricity and fuel prices, equipment lifetimes and discounting of future cash flows. The specific investment cost is a simple indicator to relate costs to performance.

Cost correlations aim to estimate purchased-equipment costs of equipment from significant sizing parameters, such as expander and pump power and heat exchanger area. The required equipment sizes are calculated from the thermodynamic cycle and equipment models introduced previously.

The purchased-equipment costs of evaporator and condenser are estimated based on the respective heat transfer area A_{HEX} using the correlation of Jaric et al. (2015) for stainless-steel/copper BPHEX, which was developed from recent market prices and is valid for heat exchanger sizes from 0.1 to 75 $\mathrm{m^2}$:

$$C_{\mathrm{PEC,HEX}} = 832\,€ \left(\frac{A_{\mathrm{HEX}}}{\mathrm{m^2}}\right)^{0.637} \tag{6}$$

The expander purchased-equipment costs are estimated from market data on small-scale refrigeration scroll compressors (Olympios et al., 2021). Since expander designs are typically based on corresponding compression machines, the costs are assumed to be similar. The data includes 55 machines with nominal powers ranging from 2.6 to 11 kW and volumetric flowrates of $2{\cdot}10^{-3}$ to $2{\cdot}10^{-2}$ $\mathrm{m^3/s}$. From the available data, the following correlation to calculate the expander costs based on the volumetric flowrate was developed:

$$C_{\mathrm{PEC,exp}} = 294{,}000\,£ \frac{\dot{V}}{\mathrm{m^3/s}} + 695\,£. \tag{7}$$

The compressor cost data includes the electric motors, which are assumed to have similar costs as generators. Therefore, the expander costs calculated from Eq. (7) are assumed also to include the generator costs.

Finally, the costs of the fluid pump are estimated from the shaft power $\dot{W}_{\mathrm{pump}}$ and the maximum pressure p using the correlation of Turton et al. (2012), assuming a positive displacement pump made from cast iron:

$$\log\left(C_{\mathrm{p}}^{0}\right) = 3.47771 + 0.1350\log\left(\dot{W}_{\mathrm{pump}}\right) + 0.1438\left(\log\left(\dot{W}_{\mathrm{pump}}\right)\right)^2, \tag{8}$$

$$\log(F_P) = \begin{cases} 0 & \text{if } p < 10 \\ -0.245382 + 0.259016\log(P) & \text{if } 10 \le P \le 100 \\ -0.01363(\log(P))^2 & \end{cases} \quad (9)$$

$$C_{PEC,pump} = C_p^0(1.89 + 1.35F_P). \quad (10)$$

All values are converted to Pound Sterling, using conversion factors of 0.89 €/£ and 0.80 $/£, the approximate averages in 2019 (Pound Sterling Live, 2025). The Chemical Engineering Plant Costing Index (CEPCI) is used to approximately account for inflation, converting all equipment costs to 2019 levels.

In line with Schilling et al. (2017a), the purchased-equipment costs are multiplied by a factor accounting for additional costs associated with, e.g., planning, installation, and commissioning to determine the total capital investment C_{TCI}:

$$C_{TCI} = 3.7\left(C_{PEC,exp} + C_{PEC,pump} + C_{PEC,evap} + C_{PEC,cond}\right). \quad (11)$$

Finally, specific investment costs C_{SIC} are calculated as ratio of total capital investment to net power output $\dot{W}_{net}$:

$$C_{SIC} = \frac{C_{TCI}}{\dot{W}_{net}}. \quad (12)$$

3. Experimental methods and model validation

Data from a test facility for the experimental investigation of small-scale ORC systems is used to develop and validate the thermodynamic models. Another purpose of the experimental data set is to select the most appropriate heat transfer correlations for the BPHEXs for this specific application.

The experimental facility and data collection methodology is described by Unamba et al. (2019). Fig. 2 shows a schematic diagram of the ORC system test facility, including auxiliary fluid loops. The main equipment is a semi-hermetic scroll expander with a built-in volume ratio of 3.5 and a displacement volume of 14.5 m^3. The expander can operate at up to 3600 rpm to generate a nominal power of 1 kW. The expander shaft is coupled to a generator. Variable resistors allow to vary the generator load and therefore the operating point of the expander. An electric oil heater with a capacity of 18 kW serves as heat source. The evaporator is a SWEP B12Lx18 BPHEX with a heat transfer area of 0.45 m^2. An Alfa Laval CB60–30H BPHEX with an area of 1.62 m^2 is installed as condenser. A mains water loop serves as heat sink. The working fluid is pumped by a Fluid-o-Tech TMFRSS051A rotary-vane pump with a maximum effective power of 250 W, which reaches a maximum volume flow of 220 L/h and a maximum pressure difference of 16 bar for water at 20 °C. R245fa, pentafluoropropane $CF_3CH_2CHF_2$, is used as working fluid, which is a common working fluid for ORC systems as it is non-ozone depleting, non-toxic and non-flammable. However, R245fa has a high global warming potential of 1030 (Honeywell International Inc., 2019). As shown in Fig. 2, the test facility is equipped with a multitude of thermocouples, pressure transducers and flow meters to monitor and log the operation. Additionally, power meters measure the power produced and the pump's consumption.

The experimental data set used for this study consists of 131 steady-state operating points. The heat source temperature was varied between 100 °C and 140 °C, with a constant thermo-oil mass flowrate of 0.5 kg/s. The working fluid mass flowrate was varied between 0.017 kg/s and 0.049 kg/s. The cooling water had a constant flowrate of 0.4 kg/s and an inlet temperature of 19 °C, resulting in an approximately constant condensation pressure of 1.5 bar. The evaporation pressure, however, varied between 5 bar and 12 bar. The generator resistance and therefore the expander speed was also varied. The measured power output was in the range from 150 to 650 W.

Experimental measurements were made using T-type thermocouples with error limits of ±1 K or ±0.75 %, pressure transducers with an accuracy of ±0.25 %, a Coriolis flow meter with an accuracy of ±0.1 %, and a power analyser with an accuracy of ±0.05 %. These potential measurement uncertainties are neglected in the analysis presented here, as they are small compared to all other uncertainties.

Several heat transfer correlations are considered for single-phase

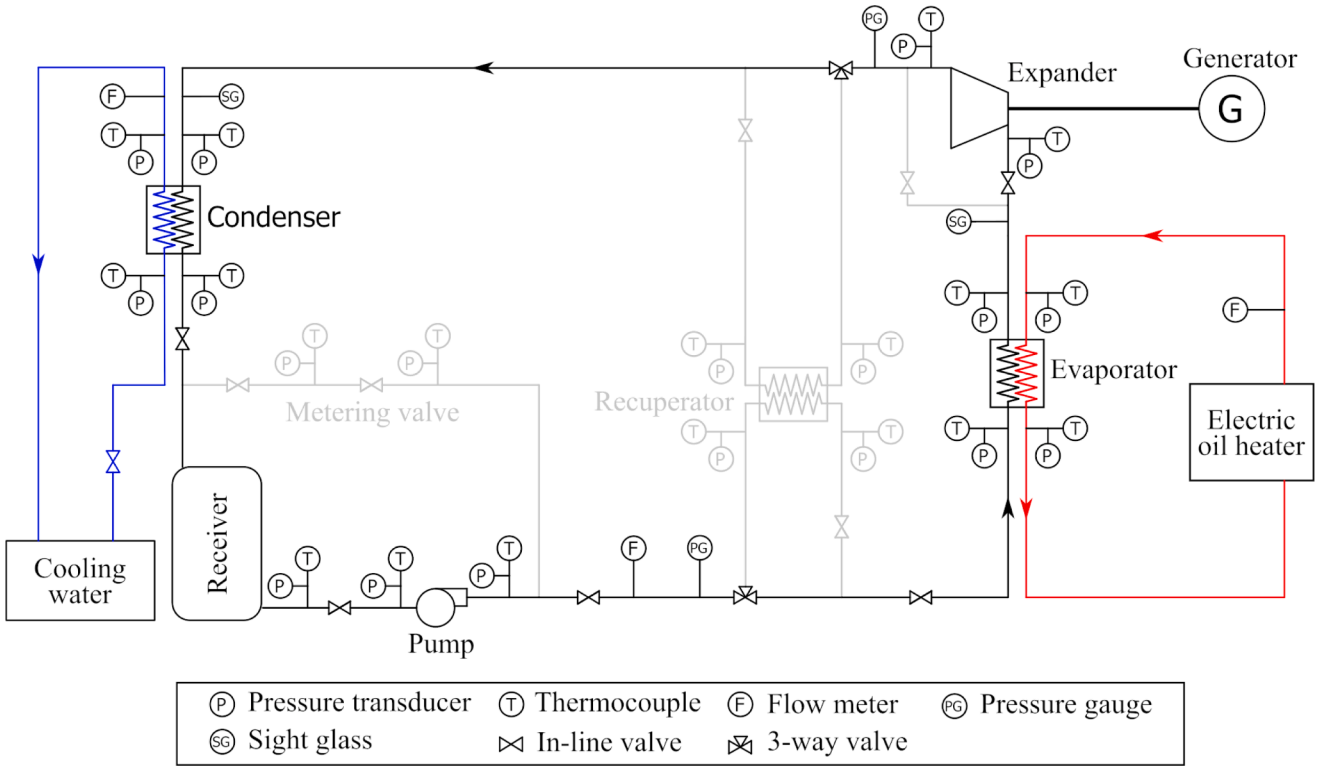

Fig. 2. Schematic diagram of the ORC system test facility, showing the installed equipment and sensors. Adapted from Unamba et al. (2019).

heat transfer, evaporation, and condensation in BPHEXs, and the most appropriate ones for the given application were selected based on the experimental data. Details on the methodology are provided in Section S7 in the supplementary information. With the best-performing heat transfer correlations, the evaporator area is predicted across all experimental data points with a root mean square error of 16 %. On average, the area is underestimated by 0.02 m^2, the standard deviation is 0.07 m^2. The root mean square error of the condenser area is only 9 %, but the area is on average underestimated by 0.13 m^2. The standard deviation of the error in the condenser area prediction is 0.06 m^2.

Finally, the experimental data is used to check the prediction accuracy of the ORC system model. Inputs are the four optimisation variables p^{r}_{evap}, p^{r}_{cond}, $\dot{m}_{wf}$ and ΔT_{sh} (see Section 2.1). The calculated powers are then compared to the corresponding experimentally measured values, as shown in Fig. 3. The expander power tends to get slightly overestimated for operating points with a high power output, while the pump power is underestimated. However, most data points are described within two standard deviations, i.e., 95 % of model errors are expected to be between −10 % and +17 % for the expander, and −14 % to +5 % for the pump. Overall, the error in the predicted net power output from the ORC system is between −13 % and +23 % in 95 % of the cases. The model error increases with increasing heat source temperatures, indicating that modelling heat losses can potentially improve the accuracy of the model significantly.

To further validate the ORC model at different scales, Fig. 3 also shows the error in the predicted power output compared to the experimental data of Yang et al. (2017), who designed and tested a geothermal ORC system with a maximum heat source temperature of 92 °C and a maximum power output of 160 kW. Similarly to our industrial case study presented below (see Table 3), these values were obtained assuming a fixed isentropic efficiency of the expander, which was set to 78 %, the average value measured during the experimental campaign. The figure shows that the errors of the large-scale system are in the same range as the ones obtained from our small-scall ORC system test facility, thus supporting the suitability of our approach.

4. Quantification and modelling of uncertainties

One key contribution of this work is the estimation of various uncertainties associated with the system and working fluid optimisation. This includes using an experimentally validated process model and accounting for the model uncertainties. For the thermo-economic CAMPD optimisation framework, uncertainties are introduced at every step from the molecular level to the plant economics level, as shown in Fig. 4.

4.1. Uncertainties in thermophysical fluid properties

Calculating thermophysical fluid properties from the molecular structure using PC-SAFT, as introduced in Section 2.2, is associated with various uncertainties. Typically, the three PC-SAFT parameters required for non-associating, unpolar molecules, m, σ and ε/k, are fitted to experimental data for the saturated liquid density ρ_L and the saturated vapour pressure p^{sat} of the relevant fluid. This parametrisation incurs two sources of uncertainty: the experimental data is subject to measurement errors, and the fitting function is unable to perfectly replicate every single data point. If GC-methods are used, another source of uncertainty is introduced: the aggregation of molecular PC-SAFT parameters from functional-group PC-SAFT parameters. Since experimental data are only available for molecules rather than functional groups, the aggregation of the functional-group parameters and the uncertainty associated with them is an inherent part of parameter fitting.

To the best of the authors' knowledge, no data on the uncertainty of functional-group SAFT parameters is available in literature. Frutiger et al. (2017) determined distributions of the PC-SAFT parameters of cyclopentane but did not consider other fluids or functional groups. Aouichaoui et al. (2022) used neural networks to estimate uncertainties in critical properties which are important for some equations of state. They then developed interpretable neural networks for pure component properties (Aouichaoui et al., 2023a) and combined them with GC approaches (Aouichaoui et al., 2023b), but did not investigate SAFT parameters. Sauer et al. (2014) presented a methodology to fit functional-group SAFT parameters of various organic groups and compare the accuracy of homo- and heterosegmented GC approaches. The authors provide the fitted PC-SAFT parameters of the functional groups, as well as the Percentage Average Absolute Deviation (%AAD) between the fits and the underlying experimental liquid density and vapour pressure data. %AAD values are commonly reported for the fluid properties used to fit the PC-SAFT parameter. However, deriving the uncertainties associated with other fluid properties or the PC-SAFT parameters themselves is not straightforward.

In this study, we express uncertainties related to the EOS as uncertainties of functional-group SAFT parameters. This approach ensures thermodynamically consistent results, which are not guaranteed if uncertainties are only applied to the calculated fluid properties. To estimate the uncertainties related to the PC-SAFT parameters, we use experimental liquid density and vapour pressure data from the DIPPR 801 database (Design Institute for Physical Properties, 2025) and a modified version of the bootstrap method for parameter uncertainty estimates developed by Frutiger et al. (2016a). The original bootstrap

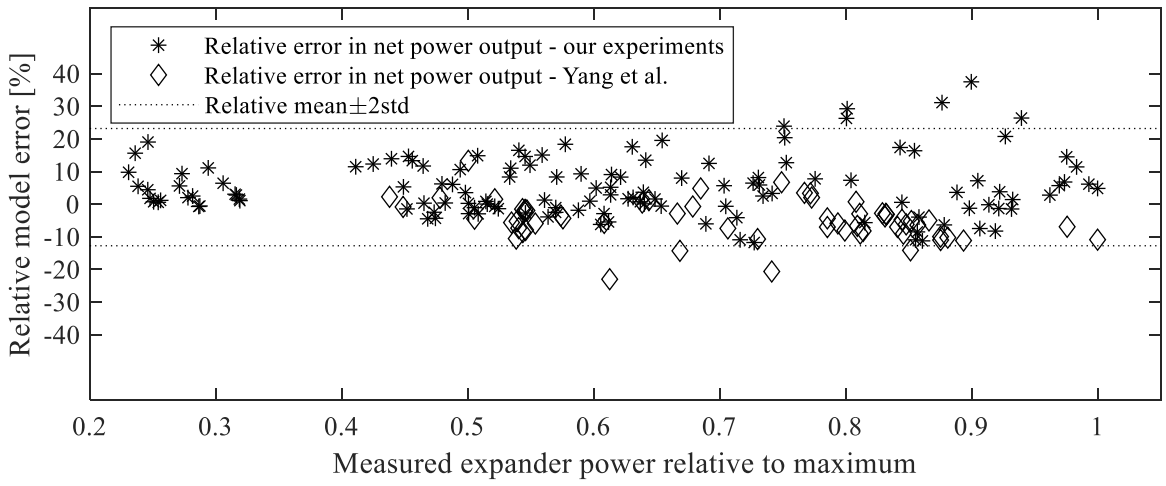

Fig. 3. Relative errors in net power output predicted by the ORC system model compared to experimentally measured values. Additionally, the range of two standard deviations (std) around the mean error is displayed. The figure also shows a comparison with experimental data obtained by Yang et al. (2017) for a 160-kW geothermal ORC system to further validate our model.

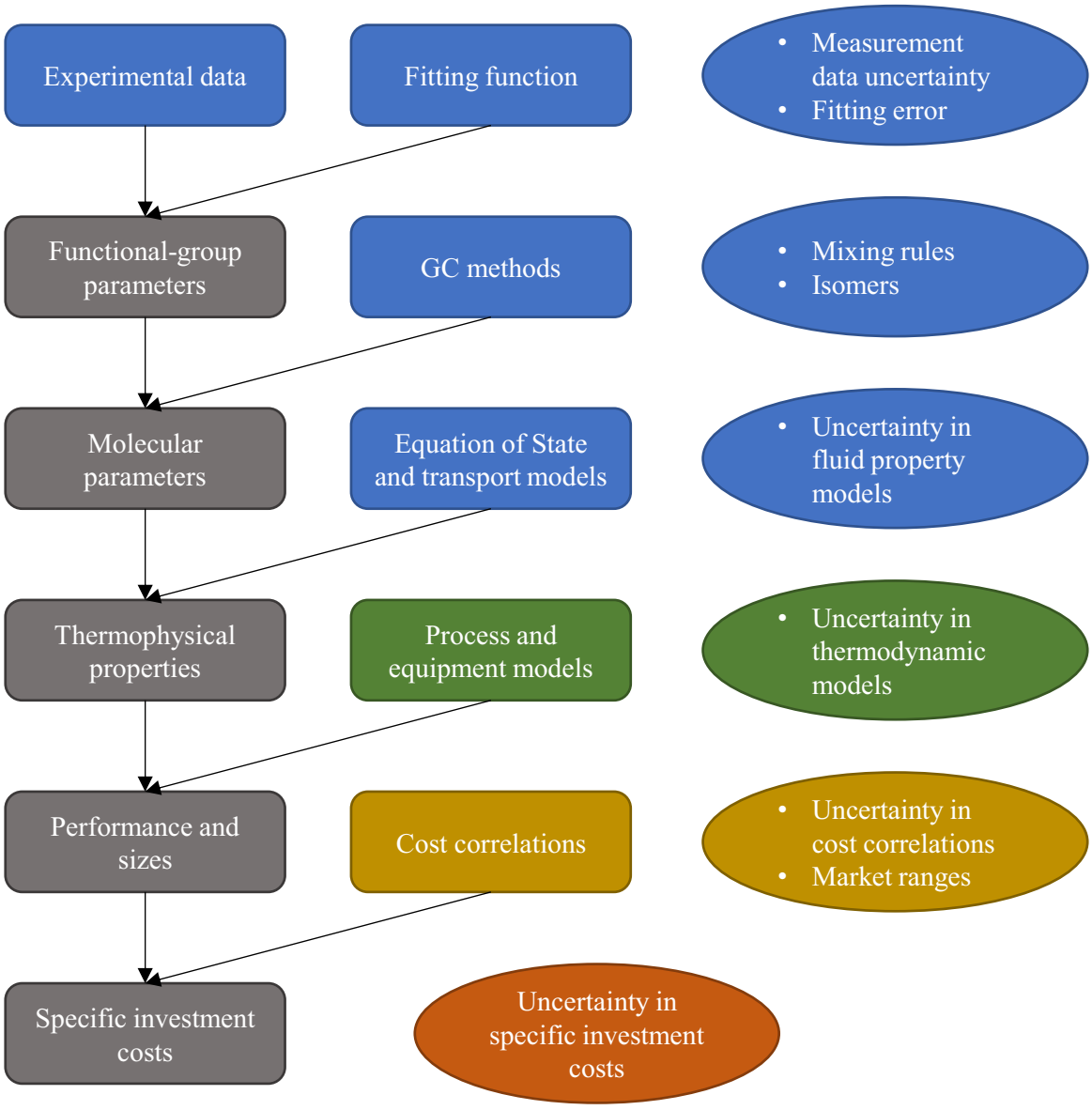

Fig. 4. Sources of uncertainties in the thermo-economic CAMPD optimisation framework, from SAFT parameters of the functional groups to specific investment costs. The top three rows represent uncertainties related to fluid properties (blue), the fourth row to uncertainties in thermodynamic cycle and equipment models (green), and the fifth row to uncertainties in equipment cost correlations (gold).

method comprises the five steps detailed below:

1. Estimate a first set of parameters from a fit to experimental data.
2. Calculate the residual errors r_i for each data point, defined as the difference between experimental value y_i^{meas} and value calculated from the initial fit y_i^{fit}:

$$r_i = y_i^{meas} - y_i^{fit}. \tag{13}$$

3. Randomly rearrange the errors to create k new synthetic data sets. For each data point, all errors have the same probability ($1/N_{Data}$) to be applied:

$$y_i(k) = y_i^{fit} + r_j. \tag{14}$$

4. Repeat the parameter fitting for each synthetic data set to obtain the final set of parameters.
5. Calculate the mean and standard deviations of the set of parameters.

Experimental liquid density and vapour pressure data of 102 linear and branched alkanes and alkenes are considered, with sizes ranging from C_4 to C_{10}. Data points with temperatures below 250 K or saturation pressures below 0.1 bar are not considered to stay close to the relevant range for the ORC system. Additionally, data points with temperatures

Table 2
Breakdown of measurement uncertainties in experimental fluid property data.

Measurement error	Number of data points	Percentage of data points	Cumulative percentage
< 0.2 %	72	2.5 %	2.5 %
< 1 %	2173	75 %	77 %
< 3 %	577	20 %	97 %
< 5 %	42	1.4 %	98 %
< 10 %	31	1.1 %	99 %
Unknown	23	0.8 %	100 %

higher than 80 % of the critical temperature are removed, because it is known that the accuracy of PC-SAFT deteriorates close to the critical point. These rules leave a total of 2918 data points for the PC-SAFT parameter regression.

A breakdown of the measurement uncertainties of the experimental data points as specified in the DIPPR 801 database is shown in Table 2. Based on these values, a measurement data uncertainty of 3 % is assumed for all further calculations, as this covers more than 95 % of all experimental data points.

To estimate PC-SAFT parameter distributions considering uncertainties in the EOS itself, the GC-method and mixing rules, as well as measurement data uncertainty and parameter fitting, the methodology

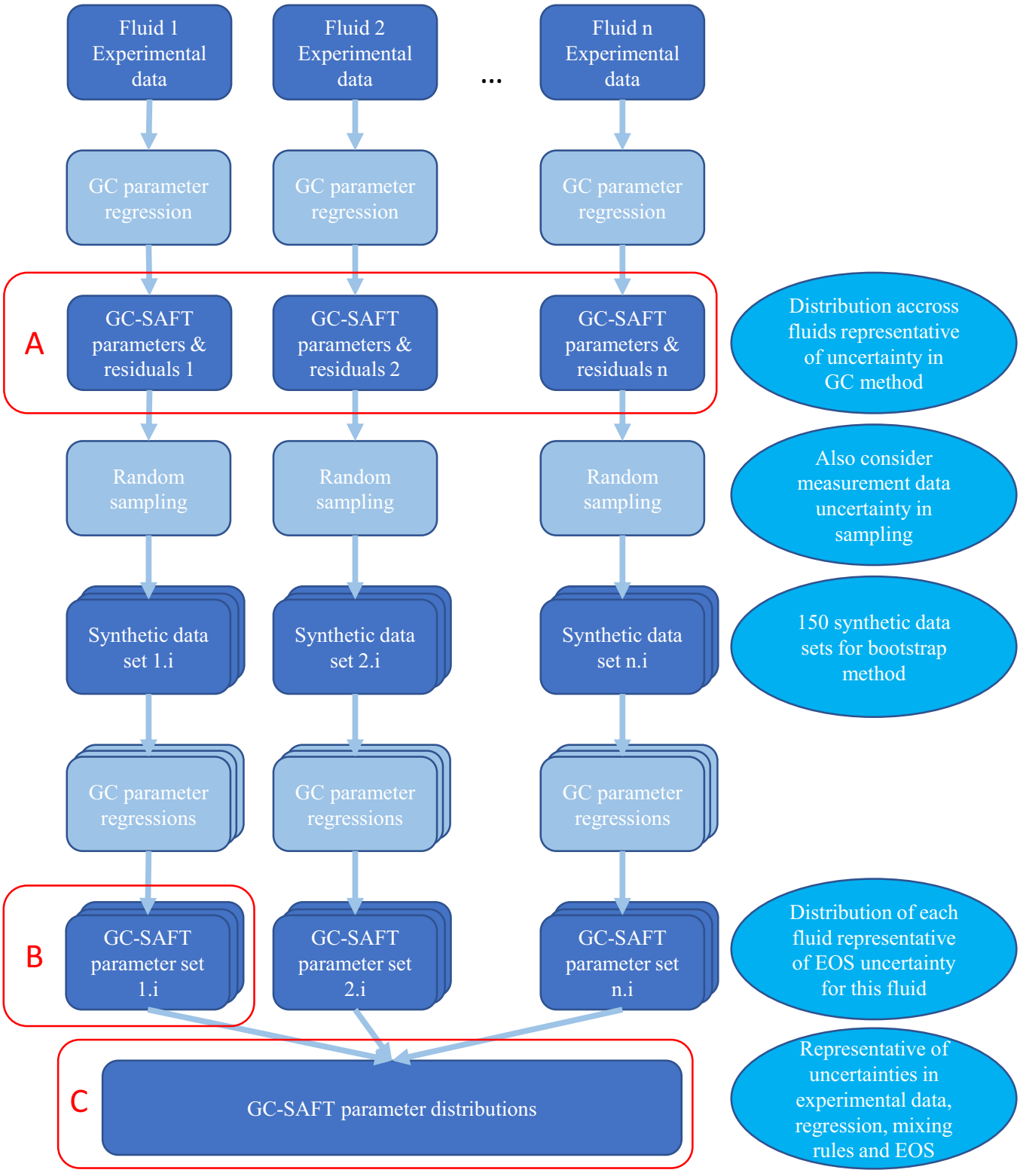

Fig. 5. Methodology to estimate uncertainties in thermophysical properties, which stem from uncertainties in the experimentally measured thermophysical fluid property data, the parameter regression, GC-methods, and mixing rules as well as the EOS.

summarised in Fig. 5 is applied, which is based on the aforementioned bootstrap method:

First, an initial parameter regression is performed for each fluid separately to identify a set of optimal functional-group PC-SAFT parameters for each. A Levenberg-Marquardt algorithm is used to minimise the residuals between the experimental liquid density and vapour pressure data and the corresponding values predicted by PC-SAFT. The molecular PC-SAFT parameters are calculated from functional-group PC-SAFT parameters using the mixing rules of Vijande et al. (2004) and then entered into the EOS to calculate thermophysical properties (see Section 2.2). The objective function proposed by Sauer et al. (2014) is used for the non-linear regression, which weighs the experimental data points based on the pressure:

$$\min\left[\frac{1}{N_\rho+N_\mathrm{p}}\left(\sum_j^{N_\rho}\left(0.5\,\frac{\rho_j^\mathrm{pred}-\rho_j^\mathrm{meas}}{\rho_j^\mathrm{meas}}\right)^2 + \sum_j^{N_\mathrm{p}}\left(\min\left(1,\ \frac{1}{5}\left(p_j^\mathrm{meas}/\mathrm{Pa}\right)^{0.15}\right)\frac{p_j^\mathrm{pred}-p_j^\mathrm{meas}}{p_j^\mathrm{meas}}\right)^2\right)\right]. \tag{15}$$

Here, N_ρ and N_p are the number of experimental data points for liquid density and vapour pressure, respectively, ρ_j the liquid density values and p_j the vapour pressure values.

It is important to note that the GC-parameter fitting problem for individual fluids is an underdetermined problem if more than one functional group is present in the fluid, which is the case for all fluids considered here. Three PC-SAFT parameters for each functional group are combined to three PC-SAFT parameters for the whole molecule, which then feed into the EOS calculations. However, infinitely many solutions exist to obtain the same whole-molecule PC-SAFT parameters from the functional-group SAFT parameters of the molecule. Here, the GC-PC-SAFT parameters determined by Sauer et al. (2014) are used as starting point for the optimisation, and the regression will converge to a local minimum solution for each fluid.

Each fluid is considered individually in the initial regression step. Therefore, each set of functional-group PC-SAFT parameters is locally-optimal for its specific fluid. Hence, the distribution of functional-group PC-SAFT parameters across the fluids (Box A in Fig. 5) is a conservative estimate of the uncertainty associated with the GC-methods and mixing rules. The distribution captures the variability in the optimal parameters for each fluid. The optimal functional-group PC-SAFT parameters determined from a regression considering multiple fluids at once would fall somewhere in the range of optimal parameters of individual fluids.

The next step is to account for the above-mentioned uncertainties in the experimentally measured thermophysical fluid property data, as well as the uncertainties associated with the EOS itself. For this purpose, a modification of the bootstrap method developed by Frutiger et al. (2016a) is applied to the individual fluids. For each fluid, GC-parameters are fitted to experimental data and thermophysical properties are predicted. Then, 150 synthetic data sets are generated for each fluid by randomly perturbing the predicted thermophysical properties. The perturbation accounts for (i) the measurement data uncertainty, estimated to be 3 % based on Table 2; and (ii) the residuals from the initial parameter fit, r_j:

$$y_{i,k}^\mathrm{syn} = \left(\alpha_{i,k}+r_j\right)y_i^\mathrm{pred} \quad \alpha_{i,k}\in F(\alpha),\ r_j\in F(r),\ k\in\{1,\cdots,150\}. \tag{16}$$

The residuals r_j are defined as the relative difference between predicted thermophysical properties from the initial parameter regression and measurement data:

$$r_j = \frac{y_j^\mathrm{pred}-y_j^\mathrm{meas}}{y_j^\mathrm{meas}}. \tag{17}$$

The measurement uncertainty perturbation factors $\alpha_{i,k}$ is drawn from a normal distribution $F(\alpha)$ with a mean value of 1 and a standard deviation of 0.03 to represent the measurement data uncertainty of 3 %. In line with the bootstrap method, a uniform distribution $F(r)$ is used for the residuals, meaning that each residual value has the same probability to be applied to each predicted value. For each of the 150 synthetic data sets, a regression is performed, yielding a total of 150 PC-SAFT parameter sets per fluid.

This methodology neglects the effect of the measurement data uncertainty on the initial parameter regression. However, by including the measurement data uncertainty in the generation of the synthetic data sets used for the bootstrap method, the influence of the measurement data uncertainties on the PC-SAFT parameter distributions is captured. The distributions of the PC-SAFT parameters per fluid (Box B in Fig. 5) estimate the uncertainties associated with the EOS and the experimental data.

Finally, all functional-group PC-SAFT parameter sets (102 fluids, 150 sets per fluid = 15,300 sets) are combined and overall distributions are determined (Box C in Fig. 5). These distributions estimate all uncertainties considered when calculating residual thermophysical properties from PC-SAFT.

Fig. 6 shows the distributions of functional-group PC-SAFT parameters from the initial fit across all fluids (Box A in Fig. 5). These distributions indicate the uncertainties associated with the GC method, as they show the variability in the locally-optimal parameter values for different fluids. It should be noted that some functional groups, such as >C<, are only present in a fraction of the considered fluids, hence the number of parameter sets for these groups is small. Some outliers are present, likely related to the identification of local minima only and the fact that the functional-group parameter fitting problem is underdetermined, as discussed above. Additionally, the distributions of the less common functional groups do not show the typical shape of normal distributions, likely due to insufficient data points. Overall, however, the functional-group PC-SAFT parameters of the considered fluids fall in similar ranges.

Fig. 7 shows the distributions of the molecular PC-SAFT parameters of n-pentane and 3-methyl-1-hexene determined from the bootstrap method (Box B in Fig. 5). These distributions capture the uncertainty in the parameter fitting, which includes the uncertainty in underlying experimental data, and uncertainties in the EOS. Such distributions were determined for all considered fluids, but only two are shown here as representative examples of a simple and a more complex organic fluid. All distributions resemble normal distributions. The PC-SAFT parameters of 3-methyl-1-hexene, the more complex fluid, show a wider distribution. However, the parameter distributions of single fluids determined by the bootstrap method (Fig. 7) show less variation than the distributions across different fluids (Fig. 6). This result suggests that the uncertainty related to the GC method and the mixing rules is larger than the one associated with the parameter fitting and the EOS itself.

To increase confidence that the distributions are representative of the overall EOS uncertainties and not just the liquid density and vapour pressure, the residuals in the enthalpy of vaporisation, a property not considered in the parameter fitting, are studied. Details are presented in Section S5 in the supplementary information. We conclude that the parameter fitting methodology is suitable for obtaining PC-SAFT parameters for the functional groups, and the distributions in GC-PC-SAFT parameters are representative of the overall EOS uncertainties.

Finally, Fig. 8 shows the aggregated functional-group PC-SAFT parameter distributions, which were obtained by combining all parameter sets (Box C in Fig. 5). These distributions are an estimate of the overall uncertainty associated with the PC-SAFT parameters. The curves represent normal distributions that were fitted to the data using the *fitdist* function in MATLAB, which estimates the standard deviation as the "square root of the unbiased estimate of the variance" (Matlab, 2024). The star symbol marks the functional-group PC-SAFT parameter values identified by Sauer et al. (2014), who used a similar GC approach but fitted the parameters for entire groups of fluids at once. The mean values of the parameter distributions identified in this work are within a

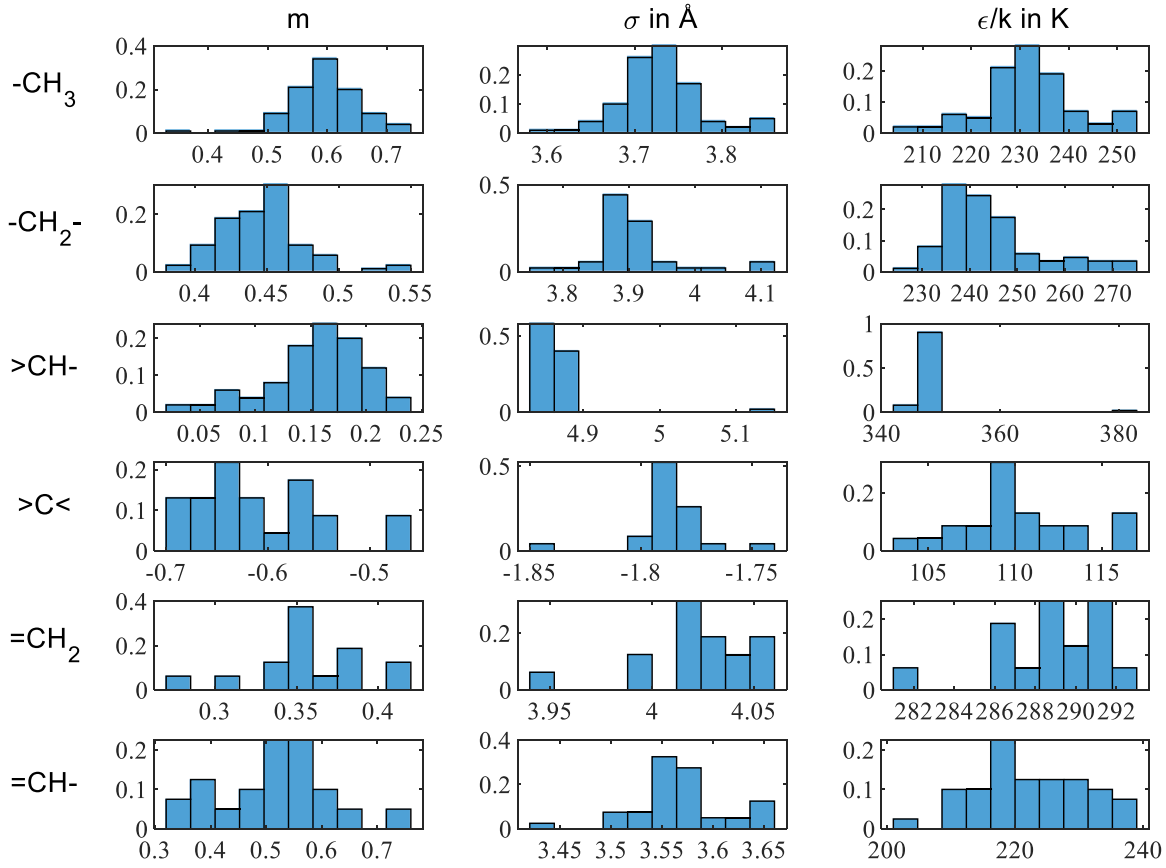

Fig. 6. Distributions A – Fitted functional-group PC-SAFT parameters across the 102 organic fluids considered for the PC-SAFT parameter regression. Each line represents a functional group, while the columns correspond to the functional-group PC-SAFT parameters.

few percent of these values, further validating the methodology used. The identified PC-SAFT parameter distributions are not perfect normal distributions. Some distributions show a second peak next to the main peak, which suggests that the distribution depends on the groups of fluids. However, for the purpose of this work, we assume that the uncertainty of the functional-group PC-SAFT parameters can be approximated by the normal distributions shown in Fig. 8.

The GC PC-SAFT parameter distributions shown in Fig. 8 account for the various uncertainties in the parameter fitting process considered here, as outlined above. For the benefit of future work on this topic, the numeric values of the means and standard deviations of these distributions are provided in Table S2 in the supplementary information. However, it is important to consider the limitations of this work, including the set of fluids used in the fitting process, when using these parameters. Considering more fluids in the parameter fitting process may result in larger uncertainties in the PC-SAFT parameters of the different functional groups, as these groups need to represent a more diverse set of fluids. Therefore, caution should be used when applying the distributions presented here in a CAMPD optimisation over a wider range of molecules. Ideally, the parameter fitting process and bootstrap method to quantify the uncertainties should be repeated considering also experimental data from the additional fluid groups of interest.

It is important to note that the GC PC-SAFT parameters are not independent but correlated, as also highlighted by Frutiger et al. (2017). More details on the correlation between parameters are provided in Section S5 in the supplementary information. Similar to the approach of Frutiger et al. (2019), the correlations are considered in the Monte Carlo sampling (see Section 4.4).

As introduced in Section 2.2, the PC-SAFT EOS only provides residual thermophysical properties. The ideal gas heat capacity is used as the reference quantity, which is calculated using the GC approach of Joback and Reid (1987). However, this approach is subject to the same uncertainties related to experimental data, the parameter fitting, and mixing rules as the estimation of the GC PC-SAFT parameters (see Fig. 4). To account for these uncertainties, the same methodology as described above for the GC PC-SAFT parameters is used to determine the distributions of the input parameters of the Joback & Reid model. Details on the ideal gas heat capacity parameter fitting, including GC parameter distributions and correlation coefficients, are provided in Section S5 in the supplementary information.

A different approach is used for the transport properties (viscosity and thermal conductivity): Based on Lötgering-Lin and Gross (2015) and Hopp and Gross (2017), who developed the correlations, and following Schilling et al. (2017a), a normal distribution with a coefficient of variation of 10 % is assumed.

4.2. Uncertainties in the ORC system model

The uncertainties in the model are estimated based on the comparison between simulated and measured performance of the ORC system test facility (see Section 3). Note that NIST REFPROP, which was used to calculate the properties of the working fluid, R245fa, is assumed to be perfectly accurate here. The REFPROP documentation for R245fa claims uncertainties below 0.1 % for liquid densities, 1 % for vapour densities, 0.35 % for vapour pressures, about 1 % for viscosities, and 1.8 % for thermal conductivities (NIST, 2018).

Fig. 3 shows that the net power output predicted by the model is on average slightly higher than the measured values, with a mean relative error of 5 %. The standard deviation of the relative error is 9 %. Therefore, the uncertainty in the predicted net power output is modelled as a normal distribution with a mean offset of 5 % and a standard deviation of 9 %. It should be noted that these values were calculated using

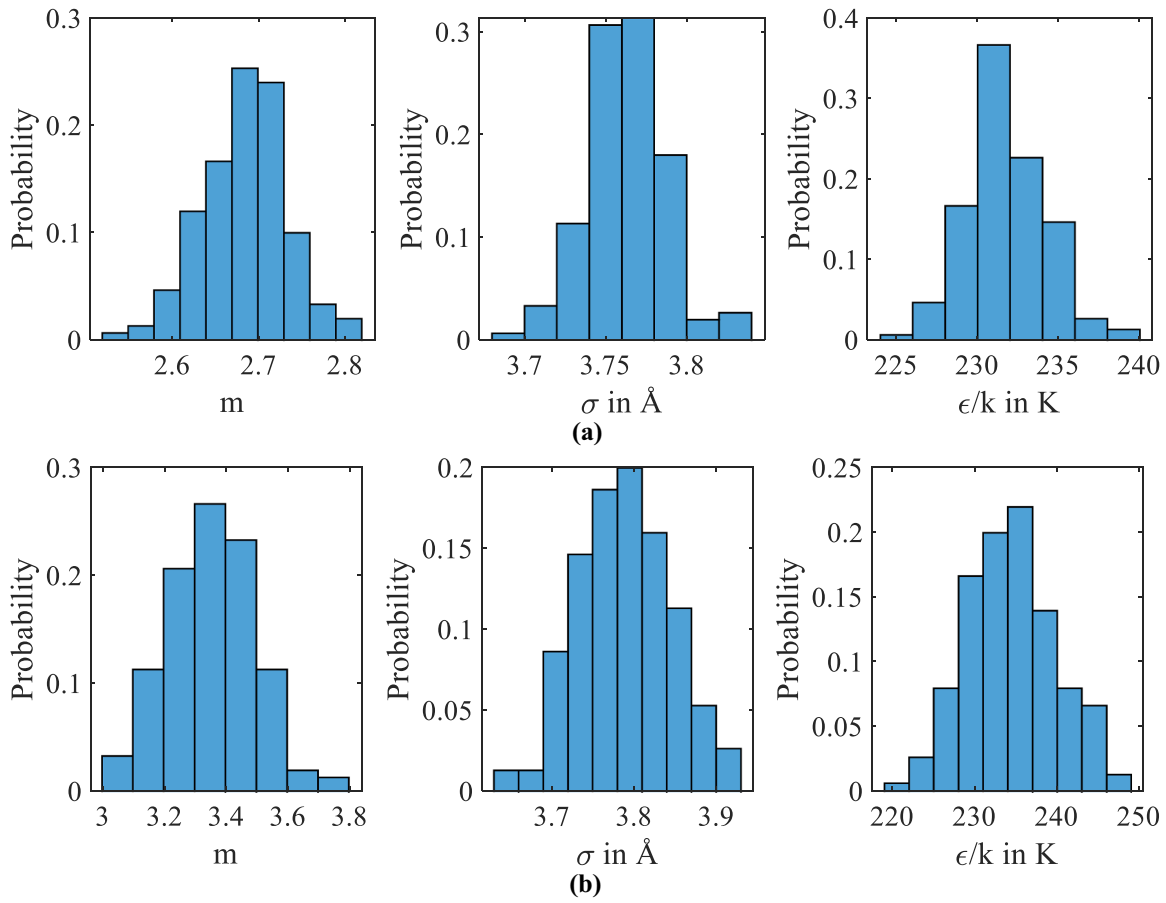

Fig. 7. Distributions B – Set of molecular PC-SAFT parameters for individual fluids as determined from the bootstrap method. Shown here are the PC-SAFT parameters m, σ and ε/k for: (a) n-pentane; and (b) 3-methyl-1-hexene as examples of a simple and a more complex fluid.

expander and pump performance maps derived from experimental data from our ORC system test facility. When modelling other systems and, e.g., relying on empirical efficiency correlation or assuming fixed isentropic efficiencies, the uncertainty in the net power output may be higher.

4.3. Uncertainties in heat transfer correlations, equipment sizing, and equipment costing

The comparison between modelled data and experimental values also shows deviations in equipment sizes, contributing to the uncertainty in equipment costs. On top of that, the correlations used to relate equipment sizes to respective costs are highly uncertain, as shown below. It is important to note, however, that these costs only indirectly impact the fluid ranking, e.g., if one fluid requires an especially large heat exchanger compared to other fluids, it is penalised more by higher heat exchanger costs. Apart from this effect, equipment cost uncertainties primarily result in a similar bias across all fluids and thus do not affect the ranking.

The heat exchanger costs are calculated from the respective heat transfer area using the correlation developed by Jaric et al. (2015) (see Eq. (6)). The authors specify that the root mean square deviation between the cost correlation and the underlying market data is 17 %. As shown in Section 3, the root mean square error of our models' evaporator HEX area prediction is 16 %, while for the condenser HEX area, it is 9 %. The two sources of uncertainty are combined using error propagation rules for independent uncertain input parameters a and b, with y as the output variable and n as a constant (Statistics How To, 2025):

$$\text{If } y = a^n \text{ then } \frac{\delta y}{|y|} = |n| \frac{\delta a}{|a|}, \tag{18}$$

$$\text{If } y = ab \text{ then } \frac{\delta y}{|y|} = \sqrt{\left(\frac{\delta a}{a}\right)^2 + \left(\frac{\delta b}{b}\right)^2}. \tag{19}$$

Following this approach, the overall standard deviations of the evaporator and condenser costs, including sizing and cost uncertainties, are estimated to be 20 % and 18 %, respectively.

The root mean square deviation between the expander cost correlation (see Eq. (7)) and the underlying data is 31 %. Unfortunately, the data on which the pump cost correlation is based is not available. We therefore assume that the uncertainty in the pump costs is the same as the uncertainty in the expander costs since both are conventional rotary machines with a mature market.

Another source of uncertainty in the investment cost calculation is the factor accounting for costs of, e.g., planning and installation (see Eq. (11)). This factor is highly uncertain and varies from project to project, but since no data is available, the uncertainty in this coefficient is not investigated further in this work. Additionally, these costs do not depend on the working fluid and therefore do not impact the ranking of different working fluids.

4.4. Methodology to consider uncertainties in the thermo-economic optimisation

The influence of uncertainties on the integrated thermo-economic system and working fluid optimisation is investigated using a Monte Carlo approach. Uncertain parameters are randomly sampled from the

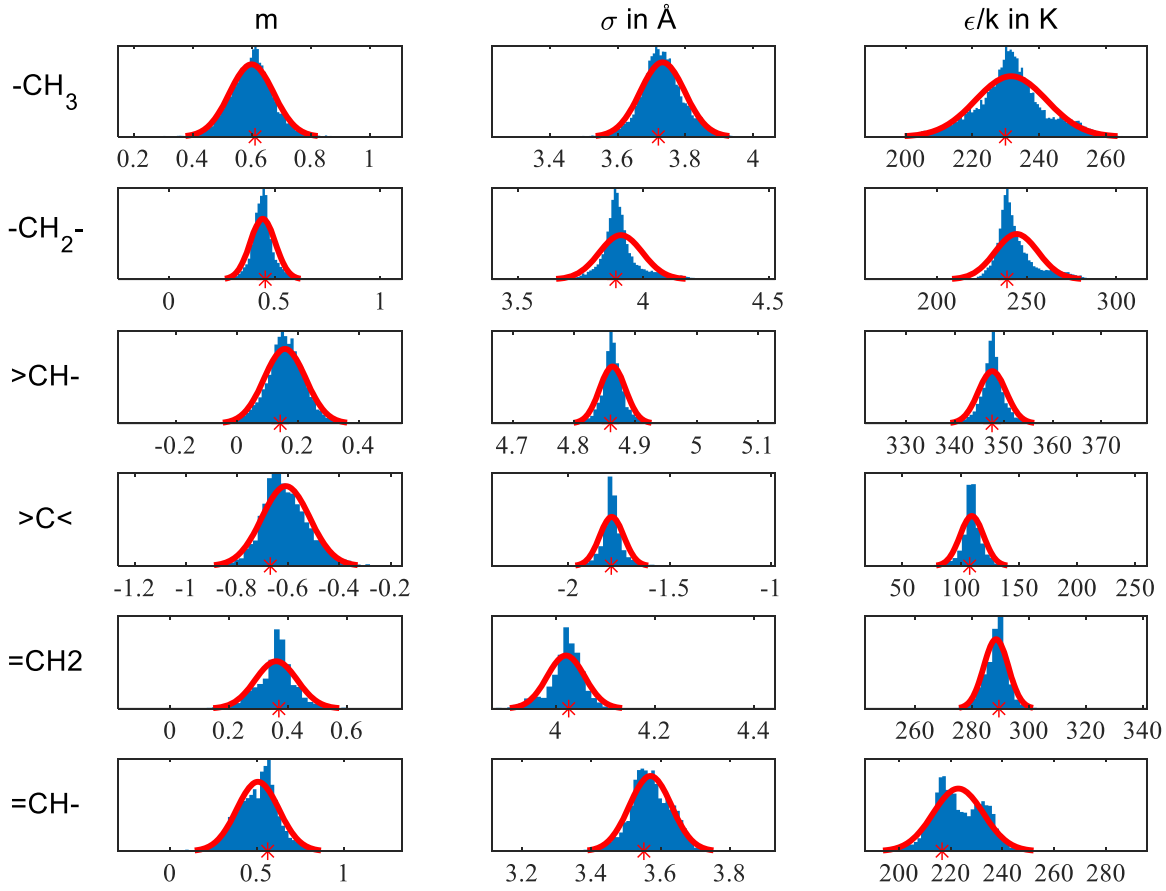

Fig. 8. Distributions C – Combination functional-group PC-SAFT parameter sets across all fluids. Plotted are also normal distributions that were fitted to the data. The star symbols indicate the parameter values identified by Sauer et al. (2014), who performed parameter regressions for a similar data set for groups of fluids.

distributions described in the previous sections, and an optimisation is performed for each set of parameter samples.

It is distinguished between uncertain parameters that influence the ranking of the working fluids and ones that do not. The former are all uncertainties related to the thermophysical property calculations as well as uncertainties in equipment size and cost calculations, while uncertainties in the overall ORC system performance only influence the value of the objective function, i.e., the specific investment costs. The latter, however, do not influence the trade-offs between working fluids.

As mentioned in Section 4.1, the functional-group PC-SAFT parameters are correlated. Therefore, a Latin hypercube sampling method that considers covariances between parameter distributions is used. The sampling is done using MATLAB's *lhsnorm* function, which performs a Latin hypercube sampling of normally distributed parameters. The function requires a positive semi-definite covariance matrix. The covariance matrix calculated from the distributions shown in Fig. 8 has some slightly negative eigenvalues, presumably because the distributions are not perfect normal distributions. The *nearestSPD* function (D'Errico, 2020) is used to perform a correction to identify the nearest positive semi-definite matrix.

The Latin hypercube sampling method is also applied to the coefficients of the ideal gas heat capacity model, accounting for correlations between parameters. The other uncertain parameters considered in this work, including transport properties and equipment costs, are assumed to be uncorrelated.

In principle, using as many samples as possible is desirable in Monte Carlo studies. However, the number of samples per study in this work is limited to 1500 due to computational limitations. Since a ranking of the 10 best ORC system designs and working fluids is generated for each sample, 1500 Monte Carlo samples require solving 15,000 MINLP optimisation problems. Despite optimising the runtime of the code, this takes over 3 weeks on a 12-core/24-thread Xeon E5–2697 processor due to the complexity of the thermodynamic cycle and equipment models and the PC-SAFT calculations as well as the difficulty to optimise non-convex MINLP problems.

5. Results and discussion

The effect of the uncertainties on the CAMPD optimisation of ORC systems is investigated in two case studies: the first one considers an ORC system similar to the test facility described in Section 3, while the second one considers an industrial application. The focus here lies on the industrial application, as it is more relevant to the deployment of ORC systems in practice. The experimental facility is quite small, with a nominal expander power of 1 kW. Results from the CAMPD optimisation of that system are provided in Section S3 in the supplementary information, while here the results from the industrial case study are

Table 3
Key parameters of the industrial case study.

Parameter	Value
Heat source fluid	Water
Heat source temperature	150 °C
Heat source pressure	10 bar
Heat source mass flowrate	1 kg/s
Heat sink fluid	Water
Heat sink temperature	15 °C
Heat sink pressure	1 bar
Heat sink mass flowrate	17.5 kg/s
Pump isentropic efficiency	0.75 (constant)
Expander isentropic efficiency	0.8 (constant)

presented. Uncertainties in fluid properties and equipment costs translate directly to the industrial case study, while model uncertainties may vary due to the different scale of the ORC system. However, for this study, we assume that the uncertainties determined in Section 3 are transferrable to the industrial case study.

The parameters for the industrial case study, summarised in Table 3, were taken from Schilling et al. (2017a). All mass flowrates were scaled by a factor of 1:10 to stay close to the experimentally validated range such that the uncertainties in thermodynamic models determined in Section 4 are still applicable.

First, the CAMPD optimisation was performed without considering uncertainties to confirm the suitability of the optimisation algorithm. Details are provided Section S1 in the supplementary information. The variation in optimal specific investment costs was found to be marginal compared to the cases with considering uncertainty. Following this validation, the CAMPD optimisation is performed with considering increasingly more uncertainties: first only uncertainties in the thermodynamic equilibrium properties stemming from the EOS and parameter fitting, then uncertainties in transport parameters are included, followed by uncertainties in equipment sizing and finally also uncertainties in equipment costing.

Results from a thermodynamic optimisation of the net power output and a thermo-economic optimisation of the specific investment costs are shown in Fig. 9. The distribution of optimal specific investment costs is significantly wider compared to the case without considering uncertainties (Figure S1 in supplementary information), with values ranging from about 3450 to 4450 £/kW. It is evident that uncertainties in thermodynamic equilibrium properties substantially impact the optimisation.

Due to the uncertainties, different working fluids are identified as optimal. Fig. 9 also shows the most likely optimal working fluids. The thermodynamic optimisation runs identify propane (39 %) as most

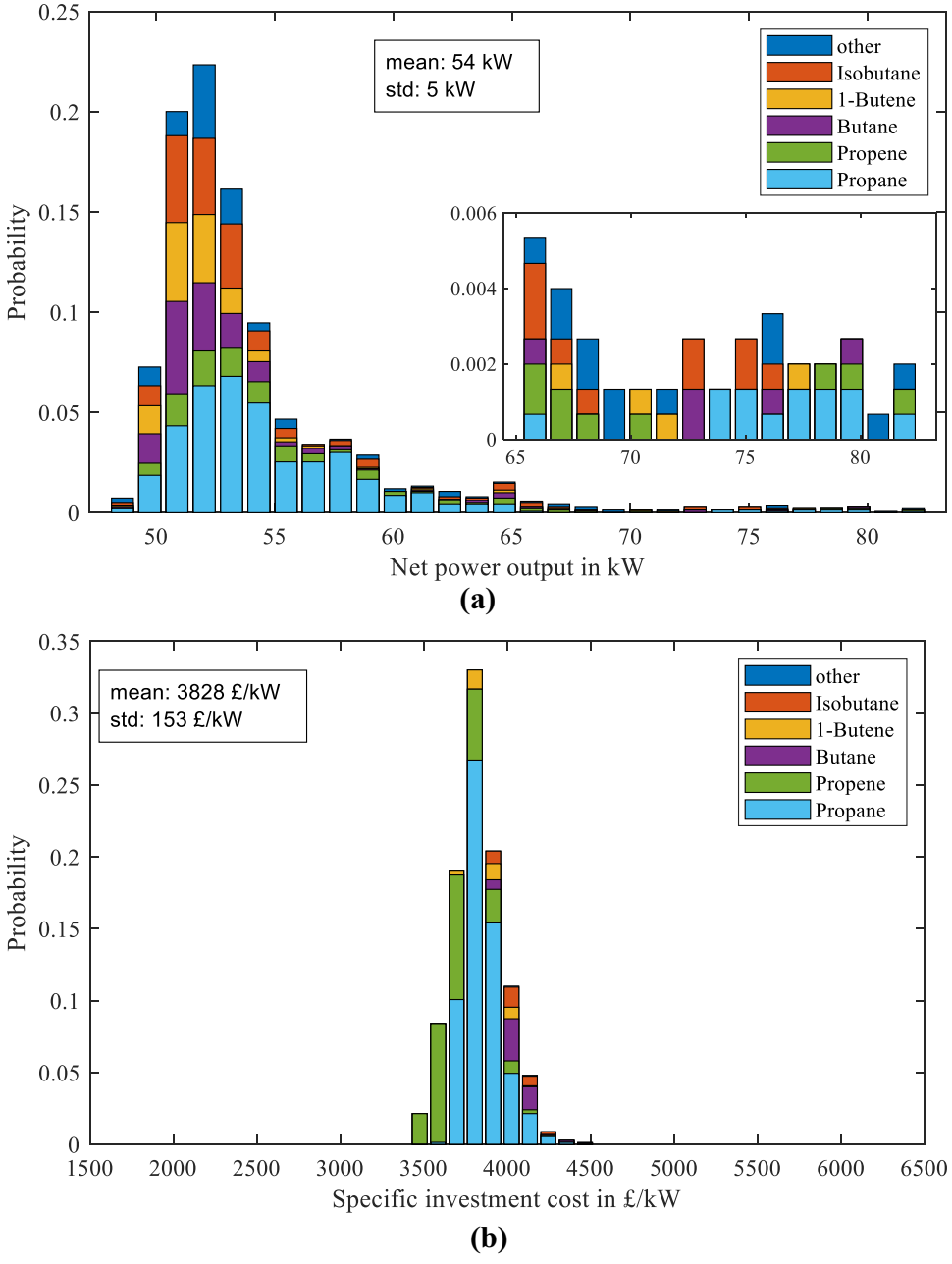

Fig. 9. Results from the CAMPD optimisation considering uncertainties in thermodynamic equilibrium properties. Shown are: (a) results from a thermodynamic optimisation maximising the net power output; and (b) results from a thermo-economic optimisation minimising specific investment costs.

likely to achieve the highest net power output, followed by isobutane (16 %), butane (14 %), 1-butene (11 %), 2-butene (10 %) and propene (10 %). All other fluids have a chance of <1 % of being the best fluid. Thus, well-performing fluids can be identified with a high probability, though it is difficult to discriminate between them. This finding is supported by looking at the 2nd-ranked fluids (isobutane – 24 %, 1-butene – 20 %, butane – 15 %, propane – 13 %, propene – 12 %, 1-butene – 11 %) and 3rd-ranked fluids (isobutane – 21 %, butane – 19 %, 1-butene – 17 %, 2-butene – 10 %, propene – 8 %, propane – 7 %). While the order of these fluids varies, they are very likely to be the best-performing ones, and the differences in their performance are small. Thus, other considerations such as the costs of these fluids or safety aspects should be considered.

The thermo-economic optimisation shows a similar picture. Propane (60 %) is most likely to perform best, followed by propene (28 %), butane (5 %), 1-butene (4 %), isobutane (3 %), and neopentane (<1 %). Under thermodynamic equilibrium property uncertainties, the CAMPD methodology cannot provide exact values for optimal net power output and specific investment costs nor strictly distinguish between the best-performing fluids, but it is useful in identifying candidate working fluids likely to perform excellently.

In the following, more and more sources of uncertainty are considered in the CAMPD optimisation. The focus is here on the thermo-economic minimisation of specific investment cost, as transport property, equipment sizing and equipment cost uncertainties do not impact the net power output.

Fig. 10 shows the distributions of optimal specific investment costs when considering more and more uncertainties. The first thing to note is that the cost ranges identified here are close to expected values for industrial applications (Schilling et al., 2017a). The mean optimal specific investment costs remain consistent at 3810 to 3840 £/kW when adding additional uncertainties to the optimisation, which is about 100 £/kW higher than the deterministic solution (see Figure S1 in the supplementary information).

The variation in optimal specific investment costs and therefore the standard deviation (std) of the distributions on the other hand increases with more uncertainties being considered in the optimisation. Adding transport property uncertainties to equilibrium property uncertainties increases the standard deviation from 153 £/kW (Fig. 9) to 159 £/kW (Fig. 10(a)), while also considering equipment sizing uncertainties results in a further increase to 165 £/kW (Fig. 10(b)). However, these changes are marginal compared to the increase in the standard deviation when adding equipment cost uncertainties. In the latter case, the standard deviation jumps to 720 £/kW (Fig. 10(c)), with optimal specific investment costs ranging from 1700 to 6200 £/kW. These findings show that uncertainties in equipment costs are by far the most influential parameter when determining optimal specific investment costs.

Fig. 10 also shows that the most-likely optimal working fluids do not change depending on the uncertainty sources being considered. Transport property, equipment sizing and costing uncertainties only have a limited impact on the selection of optimal working fluids. In any case, propane and propene are likely to perform best, followed by butane, 1-butene and isobutane.

CAMPD optimisations considering only the uncertainties in equipment cost correlations further supports that they are the most influential parameter regarding optimal specific investment costs (see Fig. S2 in the supplementary information). Even though perfect EOSs, thermodynamic cycle and equipment models were assumed for these model runs, with a standard deviation of 690 £/kW, the distribution is almost as wide as the one considering all uncertainties (Fig. 10(c)). The optimal working fluid is propene in 82 % of cases, and propane in 17 % of cases when considering only equipment cost uncertainties. Compared to the previous cases that also consider EOS uncertainties, fewer working fluids are proposed as optimal, and the top fluid is more likely to be optimal. This finding shows that the equipment cost uncertainties have only a limited impact on the working fluid selection, while EOS uncertainties are more relevant. However, regarding the specific investment costs, equipment cost uncertainties are by far the most influential uncertain parameter.

Despite the large variation in optimal specific investment costs when considering all uncertainties, high-performing working fluids can still be identified with high probability. Propane is identified as the best working fluid in 60 % of runs, as the second-best working fluid in 29 % of runs, and as the third-best working fluid in 5 % of runs, yielding an overall probability of 94 % of being among the top 3 fluids. Propene (26 % best, 15 % second-best, 9 % third-best), butane (5 % best, 13 % second-best, 19 % third-best), 1-butene (5 % best, 12 % second-best, 19 % third-best) and isobutane (4 % best, 23 % second-best, 31 % third-best) are other promising candidates. These results are consistent with the top-performing working fluids identified by Schilling et al. (2017a), who performed a deterministic CAMPD optimisation for the same case study.

The distributions of optimal specific investment costs of the promising working fluids across the different runs, shown in Fig. 11 highlight the difficulty of discriminating between well-performing working fluids strictly. Propane and propene tend to perform best. Propane does not seem to suffer from specific parameter combinations as much as other fluids; hence, its optimal specific investment costs are significantly lower in the worst-case scenario. However, the distributions widely overlap. All these fluids are likely to be among the best-performing working fluids, and other practical considerations, such as safety concerns, commercial availability or degradation should be considered when selecting working fluids for an application.

The results show that CAMPD is well suited to identify promising working fluids even when considering various uncertainties. However, obtaining a strict ranking of working fluids and an accurate estimate of expected optimal specific investment costs is challenging and further analysis and engineering are required.

A global sensitivity analysis is performed to further quantify the impact of different uncertain input parameters on the optimal specific investment costs. The results are shown in Section S4 in the supplementary information (Figure S6). The results show that especially the expander and pump cost uncertainties have a large impact, while the impacts of uncertainties in all GC-parameters and the transport properties are small compared to equipment cost uncertainties. The PC-SAFT and ideal gas heat capacity correlation parameters of frequently occurring functional groups are more influential than those of rarely occurring functional groups.

The work presented in this paper constitutes the first attempt to quantify the different uncertainties and analyse their impact on CAMPD optimisation. As a first step, it only considers simple subcritical non-recuperated ORC systems and linear and branched alkanes and alkenes as potential working fluids. In future work, the analysis should be expanded to include different ORC systems such as recuperated and supercritical cycles, as well as more groups of working fluids. Given that the CAMPD optimisation process and the different types of uncertainties are not fundamentally different, we expect similar results for more complex ORC systems. However, this should be confirmed by further research. Additionally, the GC-parameters as well as the EOS itself may be more uncertain for less common functional groups, such that it could play a larger role overall if a more diverse set of potential working fluid molecules is considered.

6. Conclusions

A comprehensive assessment of a range of uncertainties related to an integrated thermo-economic ORC system and working-fluid optimisation has been performed, using experimentally validated thermodynamic cycle and equipment models, and the PC-SAFT EOS in a CAMPD approach. Using a bottom-up bootstrap method, uncertainties in relevant fluid equilibrium property model parameters, specifically group-contribution parameters for the PC-SAFT EOS and parameters of the Joback & Reid ideal gas heat capacity correlation, were estimated.

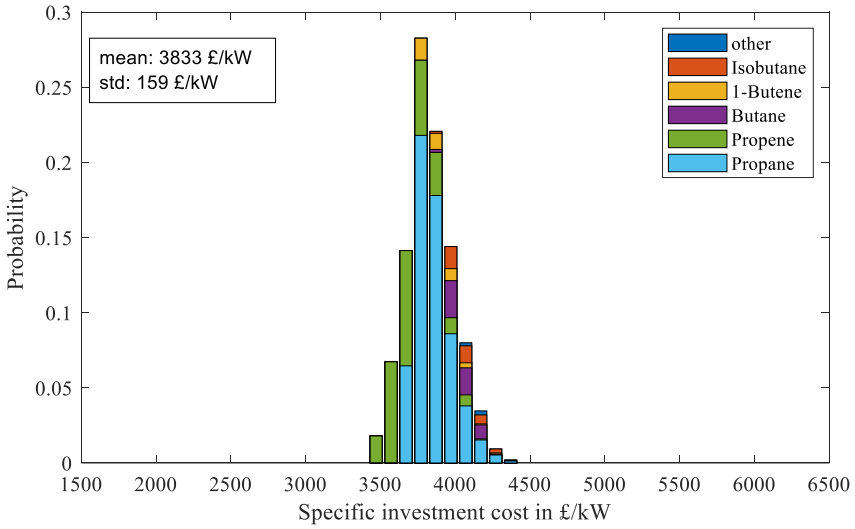

(a)

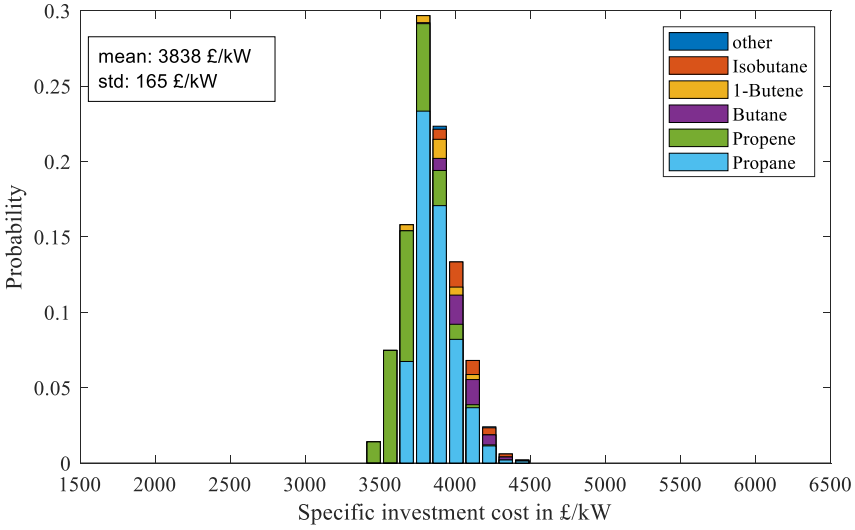

(b)

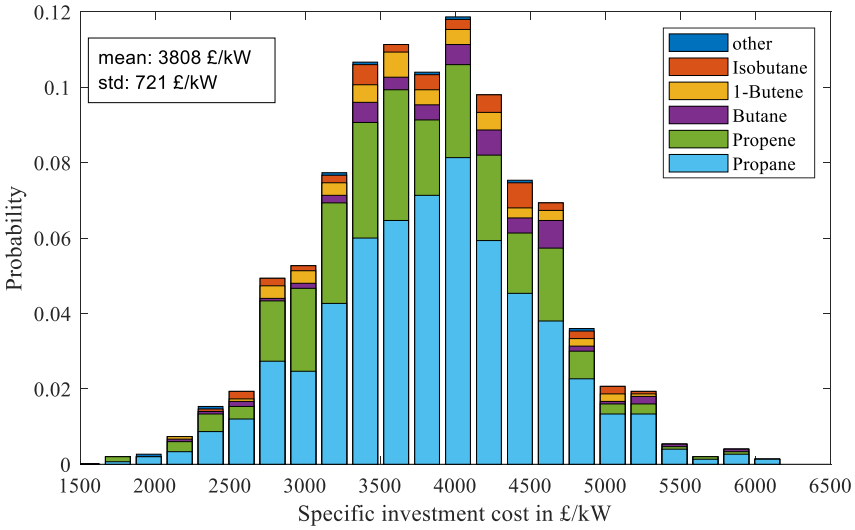

(b)

Fig. 10. Distributions of optimal specific investment costs when considering: (a) equilibrium and transport property uncertainties from the EOS; (b) equilibrium and transport property as well as equipment sizing uncertainties; and (c) equilibrium and transport property, equipment sizing and cost uncertainties.

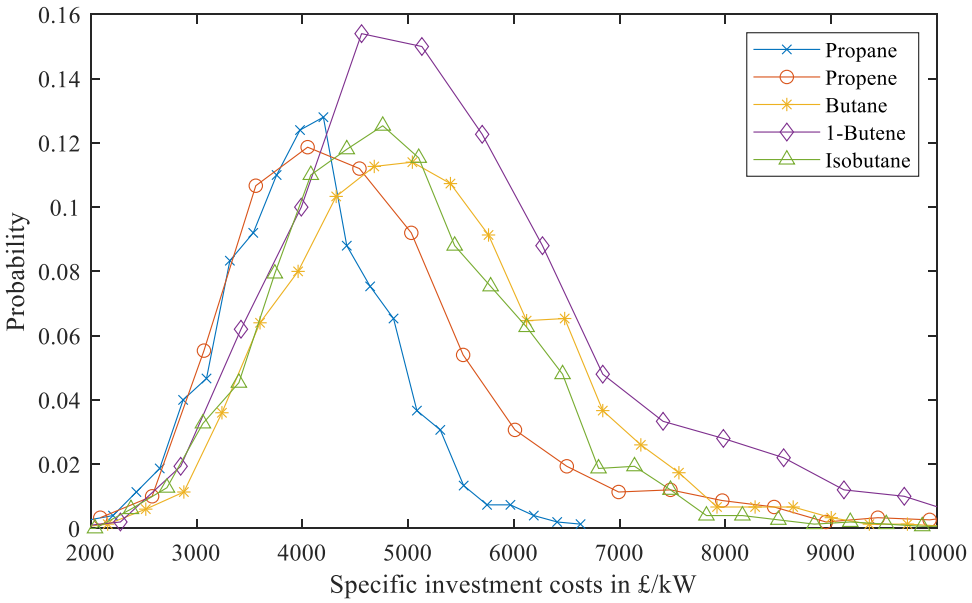

Fig. 11. Distributions of optimal specific investment costs of promising working fluids fluid when considering equilibrium and transport property, equipment sizing and cost uncertainties.

Additionally, uncertainties in transport properties, equipment sizing and equipment cost correlations were quantified. Finally, the influence of these uncertainties on the CAMPD optimisation, the optimal net power output and the specific investment costs of the ORC system were investigated using a Monte Carlo approach and the Morris method (Morris, 1991; Campolongo et al., 2007) for a global sensitivity analysis.

The CAMPD approach can identify promising working fluid candidates with high probability, even considering the various uncertainties, with propane being among the top-3 fluids in 94 % of cases. However, the absolute value of optimal specific investment cost varies widely, especially if uncertainties in equipment cost correlations are considered, which are by far the most influential uncertain parameters on specific investment costs. Considering all uncertainties, the mean optimal specific investment cost for the selected case study is 3810 £/kW, with a standard deviation of 720 £/kW (i.e., close to 20 % of the mean).

Despite all the uncertainties, the CAMPD approach can identify the best-performing working fluids with high confidence. However, strict discrimination between the best fluids is challenging, as the distributions of optimal specific investment costs widely overlap. Practical considerations and factors not included in the analysis here, such as fluid costs and availability, required pressure levels, flammability and degradation should be considered when selecting working fluids for real-world applications.

Uncertainties related to the fluid equilibrium and transport property calculations from the EOS are relevant for the working fluid selection. However, compared to the cost uncertainties, their impact on the overall optimal specific investment costs is small. When only EOS uncertainties are considered, the standard deviation in optimal specific investment costs is 160 £/kW compared to 690 £/kW when considering only equipment costing uncertainties. The results show that uncertainties should be considered when trying to estimate specific investment costs and other economic parameters of potential projects. However, the working fluid selection is robust: the best-performing molecules in the deterministic case have a high likelihood of being among the best even when considering uncertainties.

Working fluid, equipment, and system optimisation is not only relevant for ORC engines, but also for example for heat pumps (Neumaier et al., 2023; Olympios et al., 2024a, 2024b) and solvent design (Gertig et al., 2020; Lee et al., 2023). Though not explicitly considered in this study, the EOSs and methods used are the same, and uncertainties likely also play a similar role in these applications. In the future, the analysis can be expanded to other EOSs, and to include more functional groups such as aromatic groups or halogenated groups to consider a broader range of potential working fluids.

CRediT authorship contribution statement

Matthias Mersch: Writing – original draft, Visualization, Software, Methodology, Investigation, Formal analysis, Data curation. **Dominik Tillmanns:** Writing – review & editing, Supervision, Methodology, Investigation. **Paul Sapin:** Writing – review & editing, Supervision, Methodology, Investigation. **Johannes Schilling:** Writing – review & editing, Validation, Supervision, Methodology, Investigation. **André Bardow:** Writing – review & editing, Supervision, Resources, Methodology, Funding acquisition, Conceptualization. **Christos N. Markides:** Writing – review & editing, Supervision, Resources, Methodology, Funding acquisition, Conceptualization.

Declaration of competing interest

The authors declare that they have no known competing financial interests or personal relationships that could have appeared to influence the work reported in this paper.

Acknowledgements

This work was supported by the UK Engineering and Physical Sciences Research Council (EPSRC) [grant numbers EP/R045518/1 and EP/P004709/1]. Data supporting this publication can be obtained on request from cep-lab@imperial.ac.uk. For the purpose of Open Access, the authors have applied a CC BY public copyright licence to any Author Accepted Manuscript version arising from this submission.

Supplementary materials

Supplementary material associated with this article can be found, in the online version, at doi:10.1016/j.compchemeng.2025.109151.

Data availability

Data will be made available on request.

References

Alfa Laval, What is the ideal pressure drop to specify for gasketed plate heat exchangers in HVAC applications?, 2025 https://www.alfalaval.com/globalassets/documents/industries/hvac/save-now-save-later_what-is-the-ideal-pressure-drop-to-specify-for-gasketed-plate-heat-exchangers-in-hvac-applications.pdf.

Andreasen, J.G., Larsen, U., Knudsen, T., Pierobon, L., Haglind, F., 2014. Selection and optimization of pure and mixed working fluids for low grade heat utilization using organic Rankine cycles. Energy 73, 204–213. https://doi.org/10.1016/j.energy.2014.06.012.

Aouichaoui, A.R.N., Mansouri, S.S., Abildskov, J., Sin, G., 2022. Uncertainty estimation in deep learning-based property models: graph neural networks applied to the critical properties. AIChE Journal 68 (6), 17696. https://doi.org/10.1002/aic.17696.

Aouichaoui, A.R.N., Fan, F., Abildskov, J., Sin, G., 2023a. Application of interpretable group-embedded graph neural networks for pure compound properties. Comput Chem Eng 176, 108291. https://doi.org/10.1016/j.compchemeng.2023.108291.

Aouichaoui, A.R.N., Fan, F., Mansouri, S.S., Abildskov, J., Sin, G., 2023b. Combining group-contribution concept and graph neural networks toward interpretable molecular property models. J. Chem. Inf. Model. 63 (3), 725–744. https://doi.org/10.1021/acs.jcim.2c01091.

Baird Z., Pc-Saft. 2020. https://github.com/zmeri/PC-SAFT.

Bao, J., Zhao, L., 2013. A review of working fluid and expander selections for organic Rankine cycle. Renew. Sustain. Energy Rev. 24, 325–342. https://doi.org/10.1016/j.rser.2013.03.040.

Bardow, A., Steur, K., Gross, J., 2010. Continuous-molecular targeting for integrated solvent and process design. Ind. Eng. Chem. Res. 49 (6), 2834–2840. https://doi.org/10.1021/ie901281w.

Bell, I.H., Wronski, J., Quoilin, S., Lemort, V., 2014. Pure and pseudo-pure fluid thermophysical property evaluation and the open-source thermophysical property library CoolProp. Ind. Eng. Chem. Res. 53 (6), 2498–2508. https://doi.org/10.1021/ie4033999.

Bogaert, R., Böles, A., 1995. Global performance of a prototype brazed plate heat exchanger in a large reynolds number range. Exp. Heat Transf. 8 (4), 293–311. https://doi.org/10.1080/08916159508946508.

Bowskill, D.H., Tropp, U.E., Gopinath, S., Jackson, G., Galindo, A., Adjiman, C.S., 2020. Beyond a heuristic analysis: integration of process and working-fluid design for organic Rankine cycles. Mol. Syst. Des. Eng. 5 (2), 493–510. https://doi.org/10.1039/C9ME00089E.

Campolongo, F., Cariboni, J., Saltelli, A., 2007. An effective screening design for sensitivity analysis of large models. Environ. Model. Softw. 22 (10), 1509–1518. https://doi.org/10.1016/j.envsoft.2006.10.004.

Chapman, W.G., Gubbins, K.E., Jackson, G., Radosz, M., 1989. SAFT: equation-of-state solution model for associating fluids. Fluid. Phase Equilib. 52, 31–38. https://doi.org/10.1016/0378-3812(89)80308-5.

Chatzopoulou, M.A., Lecompte, S., De Paepe, M., Markides, C.N., 2019. Off-design optimisation of organic Rankine cycle (ORC) engines with different heat exchangers and volumetric expanders in waste heat recovery applications. Appl. Energy 253, 113442. https://doi.org/10.1016/j.apenergy.2019.113442.

Chen, H., Goswami, D.Y., Stefanakos, E.K., 2010. A review of thermodynamic cycles and working fluids for the conversion of low-grade heat. Renew. Sustain. Energy Rev. 14 (9), 3059–3067. https://doi.org/10.1016/j.rser.2010.07.006.

Chisholm, D., Wanniarachchi, A.S., 1991. Layout of plate heat exchangers. ASME/JSME Therm Eng Jt Conf 433-438.

D'Errico, J., 2020. nearestSPD. MATLAB Central File Exchange.

Delgado-Torres, A.M., García-Rodríguez, L., 2010. Analysis and optimization of the low-temperature solar organic rankine cycle (ORC). Energy Convers. Manage 51 (12), 2846–2856. https://doi.org/10.1016/j.enconman.2010.06.022.

Deppmann, R.L., 2025. News and Information. Velocity Limits in Gasketed Plate Heat Exchangers – Part 4. https://www.deppmann.com/blog/monday-morning-minutes/velocity-limits-gasketed-plate-heat-exchangers-part-4/.

Design Institute for Physical Properties, 2025. DIPPR Project 801 - Full Version. Design Institute for Physical Property Research/AIChE.

Drescher, U., Brüggemann, D., 2007. Fluid selection for the Organic Rankine Cycle (ORC) in biomass power and heat plants. Appl. Therm. Eng. 27 (1), 223–228. https://doi.org/10.1016/j.applthermaleng.2006.04.024.

Emadi, M.A., Chitgar, N., Oyewunmi, O.A., Markides, C.N., 2020. Working-fluid selection and thermoeconomic optimisation of a combined cycle co-generation dual-loop organic Rankine cycle (ORC) system for solid oxide fuel cell (SOFC) waste-heat recovery. Appl. Energy 261, 114384. https://doi.org/10.1016/j.apenergy.2019.114384.

Freeman, J., Hellgardt, K., Markides, C.N., 2017. Working fluid selection and electrical performance optimisation of a domestic solar-ORC combined heat and power system for year-round operation in the UK. Appl. Energy 186, 291–303. https://doi.org/10.1016/j.apenergy.2016.04.041.

Frutiger, J., Marcarie, C., Abildskov, J., Sin, G., 2016a. A comprehensive methodology for development, parameter estimation, and uncertainty analysis of group contribution based property models—An application to the heat of combustion. J. Chem. Eng. Data 61 (1), 602–613. https://doi.org/10.1021/acs.jced.5b00750.

Frutiger, J., Andreasen, J., Liu, W., Spliethoff, H., Haglind, F., Abildskov, J., Sin, G., 2016b. Working fluid selection for organic rankine cycles – Impact of uncertainty of fluid properties. Energy 109, 987–997. https://doi.org/10.1016/j.energy.2016.05.010.

Frutiger, J., Bell, I., O'Connell, J.P., Kroenlein, K., Abildskov, J., Sin, G., 2017. Uncertainty assessment of equations of state with application to an organic Rankine cycle. Mol. Phys. 115 (9–12), 1225–1244. https://doi.org/10.1080/00268976.2016.1275856.

Frutiger, J., Zühlsdorf, B., Elmegaard, B., Abildskov, J., Sin, G., 2018. Reverse engineering of working fluid selection for industrial heat pump based on Monte Carlo sampling and uncertainty analysis. Ind. Eng. Chem. Res. 57 (40), 13463–13477. https://doi.org/10.1021/acs.iecr.7b04607.

Frutiger, J., Cignitti, S., Abildskov, J., Woodley, J.M., Sin, G., 2019. Computer-aided molecular product-process design under property uncertainties – A Monte Carlo based optimization strategy. Comput. Chem. Eng. 122, 247–257. https://doi.org/10.1016/j.compchemeng.2018.08.021.

Gani, R., 2004. Chemical product design: challenges and opportunities. Comput. Chem. Eng. 28 (12), 2441–2457. https://doi.org/10.1016/j.compchemeng.2004.08.010.

Gertig, C., Fleitmann, L., Schilling, J., Leonhard, K., Bardow, A., 2020. Rx-COSMO-CAMPD: enhancing reactions by integrated computer-aided design of solvents and processes based on Quantum chemistry. Chemie Ingenieur Technik 92 (10), 1489–1500. https://doi.org/10.1002/cite.202000112.

Gross, J., Sadowski, G., 2001. Perturbed-chain SAFT: an equation of State based on a perturbation theory for chain molecules. Ind. Eng. Chem. Res. 40 (4), 1244–1260. https://doi.org/10.1021/ie0003887.

Handagama, N.B., White, M.T., Sapin, P., Markides, C.N., 2023. Renewable and Waste-Heat Utilisation Technologies. Cambridge University Press. https://doi.org/10.1017/9781108691093.

Honeywell International Inc., Genetron® 245fa (R-245fa), 2019. https://www.honeywell-refrigerants.com/europe/product/genetron-245fa/.

Hopp, M., Gross, J., 2017. Thermal conductivity of real substances from excess entropy scaling using PCP-SAFT. Ind. Eng. Chem. Res. 56 (15), 4527–4538. https://doi.org/10.1021/acs.iecr.6b04289.

Jaric, M., Budimir, N., Rakonjac, I., Budimir, S., 2015. Manufacturing costs of gasketed and brazed plate heat exchangers, total quality management - advanced and intelligent approaches. The Eighth Int. Work. Confer. 455–461.

Joback, K.G., Reid, R.C., 1987. Estimation of pure-component properties from group-contributions. Chem. Eng. Commun. 57 (1–6), 233–243. https://doi.org/10.1080/00986448708960487.

Jones, M.N., Frutiger, J., Ince, N.G., Sin, G., 2019. The Monte Carlo driven and machine learning enhanced process simulator. Comput. Chem. Eng. 125, 324–338. https://doi.org/10.1016/j.compchemeng.2019.03.016.

Lötgering-Lin, O., Gross, J., 2015. Group contribution method for viscosities based on entropy scaling using the perturbed-chain polar statistical associating fluid theory. Ind. Eng. Chem. Res. 54 (32), 7942–7952. https://doi.org/10.1021/acs.iecr.5b01698.

Lafitte, T., Apostolakou, A., Avendaño, C., Galindo, A., Adjiman, C.S., Müller, E.A., Jackson, G., 2013. Accurate statistical associating fluid theory for chain molecules formed from Mie segments. J. Chem. Phys. 139 (15), 154504. https://doi.org/10.1063/1.4819786.

Lampe, M., Stavrou, M., Schilling, J., Sauer, E., Gross, J., Bardow, A., 2015. Computer-aided molecular design in the continuous-molecular targeting framework using group-contribution PC-SAFT. Comput. Chem. Eng. 81, 278–287. https://doi.org/10.1016/j.compchemeng.2015.04.008.

Lee, Y.S., Galindo, A., Jackson, G., Adjiman, C.S., 2023. Enabling the direct solution of challenging computer-aided molecular and process design problems: chemical absorption of carbon dioxide. Comput Chem Eng 174, 108204. https://doi.org/10.1016/j.compchemeng.2023.108204.

Lemort, V., Guillaume, L., Legros, A., Declaye, S., Quoilin, S., 2013. A comparison of piston, screw and scroll expanders for small-scale Rankine cycle systems. In: Proceedings of the 3rd international conference on microgeneration and related technologies. https://hdl.handle.net/2268/147369.

Liang, Z., Liang, Y., Luo, X., Chen, J., Yang, Z., Wang, C., Chen, Y., 2022. Superstructure-based mixed-integer non-linear programming framework for hybrid heat sources driven organic rankine cycle optimization. Appl. Energy 307, 118277. https://doi.org/10.1016/j.apenergy.2021.118277.

Linke, P., Papadopoulos, A., Seferlis, P., 2015. Systematic methods for working fluid selection and the design, integration and control of organic rankine cycles—A review. Energies 8 (6), 4755–4801. https://doi.org/10.3390/en8064755.

Matlab, fitdist, 2024. https://uk.mathworks.com/help/stats/fitdist.html#btu54g1-1.

Markides, C.N., Wang, K., 2023. Power Generation Technologies For Low-Temperature and Distributed Heat. Woodhead Publishing Series in Energy. https://doi.org/10.1016/C2018-0-03181-3.

Markides, C.N., Bardow, A., De Paepe, M., De Servi, C., Gross, J., Haslam, A.J., Lecompte, S., Papadopoulos, A.I., Oyewunmi, O.A., Seferlis, P., Schilling, J., Linke, P., Tian, H., Shu, G., 2025. Working fluid and system optimisation of organic rankine cycles via computer-aided molecular design: a review. Prog Energy Combust Sci 107, 101201. https://doi.org/10.1016/j.pecs.2024.101201.

Morris, M.D., 1991. Factorial sampling plans for preliminary computational experiments. Technometrics. 33 (2), 161–174. https://doi.org/10.1080/00401706.1991.10484804.

National Institute of Standards and Technology (NIST), REFPROP, NIST Reference Fluid Thermodynamic and Transport Properties Database (REFPROP): version 10, 2018. https://www.nist.gov/srd/refprop.

Neumaier, L., Roskosch, D., Schilling, J., Bauer, G., Gross, J., Bardow, A., 2023. Refrigerant selection for heat pumps: the compressor makes the difference. Energy Technology 11 (4), 2201403. https://doi.org/10.1002/ente.202201403.
Olympios A.V., Mersch M., Sapin P., Pantaleo A.M., Markides C.N., Library of price and performance data of domestic and commercial technologies for low-carbon energy systems. 2021. https://doi.org/10.5281/zenodo.4692648.
Olympios, A.V., Hoseinpoori, P., Markides, C.N., 2024a. Towards optimal designs of domestic air-to-water heat pumps for a net-zero carbon energy system in the UK. Cell Rep. Sustain. 1 (2), 100021. https://doi.org/10.1016/j.crsus.2024.100021.
Olympios, A.V., Sapin, P., Mersch, M., Maghrabi, A.M., Markides, C.N., 2024b. A review of recent progress in the design and integration of domestic heat pumps. Next Energy 5, 100163. https://doi.org/10.1016/j.nxener.2024.100163.
Palma-Flores, O., Flores-Tlacuahuac, A., Canseco-Melchor, G., 2015. Optimal molecular design of working fluids for sustainable low-temperature energy recovery. Comput. Chem. Eng. 72, 334–349. https://doi.org/10.1016/j.compchemeng.2014.04.009.
Pantaleo, A.M., Simpson, M., Rotolo, G., Distaso, E., Oyewunmi, O.A., Sapin, P., De Palma, P., Markides, C.N., 2019. Thermoeconomic optimisation of small-scale organic rankine cycle systems based on screw vs. piston expander maps in waste heat recovery applications. Energy Convers. Manage 200, 112053. https://doi.org/10.1016/j.enconman.2019.112053.
Papadopoulos, A.I., Stijepovic, M., Linke, P., 2010. On the systematic design and selection of optimal working fluids for organic rankine cycles. Appl. Therm. Eng. 30 (6–7), 760–769. https://doi.org/10.1016/j.applthermaleng.2009.12.006.
Papadopoulos, A.I., Stijepovic, M., Linke, P., Seferlis, P., Voutetakis, S., 2013. Toward optimum working fluid mixtures for organic rankine cycles using molecular design and sensitivity analysis. Ind. Eng. Chem. Res. 52 (34), 12116–12133. https://doi.org/10.1021/ie400968j.
Peng, D-Y, DB, Robinson, 1976. A new two-constant equation of state. Ind Eng Chem Fundam 15 (1), 59–64. https://doi.org/10.1021/i160057a011.
Pound Sterling Live, 2025 https://www.poundsterlinglive.com/.
Preißinger, M., Schwöbel, J.A.H., Klamt, A., Brüggemann, D., 2017. Multi-criteria evaluation of several million working fluids for waste heat recovery by means of Organic Rankine Cycle in passenger cars and heavy-duty trucks. Appl. Energy 206, 887–899. https://doi.org/10.1016/j.apenergy.2017.08.212.
Quoilin, S., Declaye, S., Tchanche, B.F., Lemort, V., 2011. Thermo-economic optimization of waste heat recovery organic rankine cycles. Appl. Therm. Eng. 31 (14–15), 2885–2893. https://doi.org/10.1016/j.applthermaleng.2011.05.014.
Quoilin, S., van den Broek, M., Declaye, S., Dewallef, P., Lemort, V., 2013. Techno-economic survey of Organic Rankine Cycle (ORC) systems. Renew. Sustain. Energy Rev. 22, 168–186. https://doi.org/10.1016/j.rser.2013.01.028.
Rosenfeld, Y., 1977. Relation between the transport coefficients and the internal entropy of simple systems. Phys. Rev. a 15 (6), 2545–2549. https://doi.org/10.1103/PhysRevA.15.2545.
Rosenfeld, Y., 1999. A quasi-universal scaling law for atomic transport in simple fluids. J. Phys. Condens. Matter. 11 (28), 5415–5427. https://doi.org/10.1088/0953-8984/11/28/303.
Saleh, B., Koglbauer, G., Wendland, M., Fischer, J., 2007. Working fluids for low-temperature organic Rankine cycles. Energy 32 (7), 1210–1221. https://doi.org/10.1016/j.energy.2006.07.001.
Sasol Olefins & Surfactants GmbH. Marlotherm SH: product information, 2003.
Sauer, E., Stavrou, M., Gross, J., 2014. Comparison between a Homo- and a heterosegmented group contribution approach based on the perturbed-chain polar statistical associating fluid theory equation of State. Ind. Eng. Chem. Res. 53 (38), 14854–14864. https://doi.org/10.1021/ie502203w.
Schilling, J., Tillmanns, D., Lampe, M., Hopp, M., Gross, J., Bardow, A., 2017a. From molecules to dollars: integrating molecular design into thermo-economic process design using consistent thermodynamic modeling. Mol. Syst. Des. Eng. 2 (3), 301–320. https://doi.org/10.1039/C7ME00026J.
Schilling, J., Lampe, M., Gross, J., Bardow, A., 2017b. 1-stage CoMT-CAMD: an approach for integrated design of ORC process and working fluid using PC-SAFT. Chem. Eng. Sci. 159, 217–230. https://doi.org/10.1016/j.ces.2016.04.048.
Schwöbel, J.A.H., Preißinger, M., Brüggemann, D., Klamt, A., 2017. High-throughput screening of working fluids for the organic rankine cycle (ORC) based on conductor-like screening model for realistic solvation (COSMO-RS) and thermodynamic process simulations. Ind. Eng. Chem. Res. 56 (3), 788–798. https://doi.org/10.1021/acs.iecr.6b03857.
Shah, R.K., Sekuli, D.P., 2003. Fundamentals of Heat Exchanger Design. John Wiley & Sons, Hoboken, NJ, USA. Incf.
Soave, G., 1972. Equilibrium constants from a modified Redlich-Kwong equation of state. Chem. Eng. Sci. 27 (6), 1197–1203. https://doi.org/10.1016/0009-2509(72)80096-4.
Statistics How To, 2025. Error Propagation. Propagation of Uncertainty. https://www.statisticshowto.com/statistics-basics/error-propagation/.
Stijepovic, M.Z., Linke, P., Papadopoulos, A.I., Grujic, A.S., 2012. On the role of working fluid properties in organic Rankine Cycle performance. Appl. Therm. Eng. 36, 406–413. https://doi.org/10.1016/j.applthermaleng.2011.10.057.
Struebing, H., 2011. Identifying Optimal Solvents For Reactions Using Quantum Mechanics and Computer-Aided Molecular Design. Imperial College London. https://doi.org/10.25560/9150.
Tchanche, B.F., Papadakis, G., Lambrinos, G., Frangoudakis, A., 2009. Fluid selection for a low-temperature solar organic rankine cycle. Appl. Therm. Eng. 29 (11–12), 2468–2476. https://doi.org/10.1016/j.applthermaleng.2008.12.025.
The MathWorks Inc., surrogateopt, 2021a. https://www.mathworks.com/help/gads/surrogateopt.html.
The MathWorks Inc., fmincon, 2021b. https://www.mathworks.com/help/optim/ug/fmincon.html.
Thierry, D.M., Flores-Tlacuahuac, A., Grossmann, I.E., 2016. Simultaneous optimal design of multi-stage organic rankine cycles and working fluid mixtures for low-temperature heat sources. Comput Chem Eng 89, 106–126. https://www.sciencedirect.com/science/article/pii/S0098135416300588?via%3Dihub.
Thonon, B., Bontemps, A., 2002. Condensation of pure and mixture of hydrocarbons in a compact heat exchanger: experiments and modelling. Heat Transf Eng 23 (6), 3–17. https://doi.org/10.1080/01457630290098718.
Tillmanns, D., Pell, D., Schilling, J., Bardow, A., 2022. The thermo-economic potential of ORC-based pumped-thermal electricity storage: insights from the integrated design of processes and working fluids. Energy Technology 10 (7), 2200182. https://doi.org/10.1002/ente.202200182.
Turton, R., Bailie, R.C., Whiting, W.B., Shaeiwitz, J.A., Bhattacharyya, D., 2012. Analysis, Synthesis, and Design of Chemical Processes. Prentice Hall. Fourth Edition.
Unamba, C.K., Sapin, P., Li, X., Song, J., Wang, K., Shu, G., Tian, H., Markides, C.N., 2019. Operational optimisation of a non-recuperative 1-kWe organic rankine cycle engine prototype. Appl. Sci. 9 (15), 3024. https://doi.org/10.3390/app9153024.
United Nations, 2016. The Kigali Amendment. In: The amendment to the Montreal Protocol agreed by the Twenty-Eighth Meeting of the Parties. Kigali, 10-15 October 20162016.
van Kleef, L.M.T., Oyewunmi, O.A., Markides, C.N., 2019. Multi-objective thermo-economic optimization of organic rankine cycle (ORC) power systems in waste-heat recovery applications using computer-aided molecular design techniques. Appl. Energy 251, 112513. https://doi.org/10.1016/j.apenergy.2019.01.071.
Vijande, J., Piñeiro, M.M., Bessières, D., Saint-Guirons, H., Legido, J.L., 2004. Description of PVT behaviour of hydrofluoroethers using the PC-SAFT EOS. Phys. Chem. Chem. Phys. 6 (4), 766–770. https://doi.org/10.1039/B312223A.
Wang, E.H., Zhang, H.G., Fan, B.Y., Ouyang, M.G., Zhao, Y., Mu, Q.H., 2011. Study of working fluid selection of organic rankine cycle (ORC) for engine waste heat recovery. Energy 36 (5), 3406–3418. https://doi.org/10.1016/j.energy.2011.03.041.
White, M.T., Oyewunmi, O.A., Haslam, A.J., Markides, C.N., 2017. Industrial waste-heat recovery through integrated computer-aided working-fluid and ORC system optimisation using SAFT-γ Mie. Energy Convers. Manage 150, 851–869. https://doi.org/10.1016/j.enconman.2017.03.048.
White, M.T., Oyewunmi, O.A., Chatzopoulou, M.A., Pantaleo, A.M., Haslam, A.J., Markides, C.N., 2018. Computer-aided working-fluid design, thermodynamic optimisation and thermoeconomic assessment of ORC systems for waste-heat recovery. Energy 161, 1181–1198. https://doi.org/10.1016/j.energy.2018.07.098.
Yang, Y., Huo, Y., Xia, W., Wang, X., Zhao, P., Dai, Y., 2017. Construction and preliminary test of a geothermal ORC system using geothermal resource from abandoned oil wells in the Huabei oilfield of China. Energy 140 (1), 633–645. https://doi.org/10.1016/j.energy.2017.09.013.
Zhai, H., Shi, L., An, Q., 2014. Influence of working fluid properties on system performance and screen evaluation indicators for geothermal ORC (organic Rankine cycle) system. Energy 74, 2–11. https://doi.org/10.1016/j.energy.2013.12.030.
Zhang, B., Wang, E., Meng, F., Zhang, F., Zhao, C., 2020. Prediction accuracy of thermodynamic properties using PC-SAFT for high-temperature organic rankine cycle with siloxanes. Energy 204, 117980. https://doi.org/10.1016/j.energy.2020.117980.